SOFTWARE FOR FIRST RESPONDERS ALLOWING FOR INTERPRETATION OF PORTABLE SURVEY METER RESPONSES IN RADIOLOGICAL TRIAGE DECISIONS

By

BADAL JUNEJA

A THESIS PRESENTED TO THE GRADUATE SCHOOL
OF THE UNIVERSITY OF FLORIDA IN PARTIAL FULFILLMENT
OF THE REQUIREMENTS FOR THE DEGREE OF
MASTER OF SCIENCE

UNIVERSITY OF FLORIDA

2011

To my parents, who inspired me to achieve more than I had ever dreamed of

ACKNOWLEDGMENTS

I thank my advisor, Dr. Wesley E. Bolch, for his guidance and encouragements over the last three years. Whenever I had a problem, Dr. Bolch had a solution. I would not be writing this document today without his support. I also thank Dr. Choonsik Lee and Mike Wayson for letting me generously use their codes to import the phantoms. Finally, I thank the TKC Global for their research support by a contract CDC-UF-Task134.

TABLE OF CONTENTS

page

ACKNOWLEDGMENTS 4

LIST OF TABLES 7

LIST OF FIGURES 8

LIST OF ABBREVIATIONS 9

ABSTRACT 10

CHAPTER

1 INTRODUCTION 12

2 MATERIALS AND METHODS 17

Hybrid Patient-Dependent Phantoms Representing Internally Contaminated Individuals 17
Exposure Scenarios 18
Derivation of Detector Response Functions and Count Rate Thresholds 19
Phantom Source Regions 22
Organ Source Definition 22
SSW/SSR 23
Monte Carlo Detector Models 24
Creating a Graphical User Interface 26

3 RESULTS 34

Software Output 34
Recommendations for Medical Response Based on Estimated Range of Effective Dose 36

4 DISCUSSION 44

Variation in Count Rate Threshold by Detector Type 44
Variation in Count Rate Threshold by Subject Age and Gender 45
Variation in Count Rate Threshold by Subject Weight Percentile 45
Analysis of the Monte Carlo Detector Efficiencies 46

5 CONCLUSION 54

APPENDIX

A EXCEL OUTPUT OF THE SOFTWARE 56

LIST OF REFERENCES 57

BIOGRAPHICAL SKETCH 59

LIST OF TABLES

Table		page
2-1	Height and Weight of the eleven phantoms used in this study	30
2-2	Summary of dose coefficient for Effective Dose (Sv per Bq intake) for all 21 exposure scenarios considered in this study for different age groups.	31
2-3	Source Organs and tissue modeled in the computational phantoms for each of the five radionuclides considered in this study. Organs for which the fractional uptake never exceeds 1% were not considered in modeling survey meter response functions.	32
2-4	Selection of source tissues and organs in the computational phantoms used to model radionuclide source within circulating blood of the adult male and female.	33
3-1	Representative table for time dependent count rate (in cpm) corresponding to Ir-192 Inhalation (1 micrometer AMAD and Type M solubility class) for the adult male (90^{th} weight percentile) with the Capintec Captus 3000 detector placed 100 cm away from the back of the abdomen.	38
3-2	Recommendations for medical response following radiological triage screening by radionuclide and estimated range of effective dose based on survey meter count rate measurements.	39
A-1	Excel output from the PC-based MATLAB GUI	56

LIST OF FIGURES

Figure page

2-1 The University of Florida's Hybrid Computational Phantoms representing (from left to right) 10th, 50th, and 90th weight percentile adult male and 10th, 50th, and 90th weight percentile adult female. 27

2-2 The University of Florida's Hybrid Computational Phantoms representing (from left to right) 1-year, 5-year, 10-year, 15-year (female) and 15-year (male) 50th weight percentile individuals 28

2-3 Rhinoceros models of the five detectors used in this study: A) Ludlum 44-9 GM Probe, B) Ludlum 44-2 Survey Meter, C) Canberra InSpector 1000 Survey Meter, D) Ludlum 12s Survey Meter, and E) Capintec Captus 3000. 29

3-1 The GUI created in MATLAB for easy access to data generated in this study. .. 40

3-2 Representative graph for time dependent count rate (in cpm) corresponding to Ir-192 Inhalation (1 micrometer AMAD and Type M solubility class) for the adult male (90th weight percentile) with the Capintec Captus 3000 detector placed 100 cm away from the back of the abdomen. 41

3-3 Time dependent count rate (in cpm) corresponding to Co-60 Ingestion for the adult female (90th weight percentile) with the Ludlum 44-2 detector placed (A) 30 cm and (B) 100 cm away from the back of the chest. 42

3-4 Triage condition assessment for Ir-192 Inhalation for the adult male with the Capintec Captus 3000 placed 100 cm away from the back of the abdomen reading gross count rate of (A) 225,000 cpm and (B) 1,000,000 cpm 43

4-1 Comparison of 250 mSv count rate thresholds for the four survey meters for each radionuclide exposure scenarios assuming inhalation and default particle size and solubility type: A) Am-241, B) Co-60, C) Cs-137, D) I-131, and E) Ir-192 48

4-2 Comparison of 250 mSv count rate thresholds for all the age and gender combinations evaluated in this study assuming I-131 inhalation using the the Canberra InSpector 1000 spectrometer placed 100 cm away from the back of the chest. 51

4-3 Comparison of 50 mSv count rate thresholds for the 10th, 50th, and 90th weight percentile adult male phantoms assuming Cs-137 inhalation using the Ludlum 44-2 survey probe placed at the back of the chest. 52

4-4 Comparison of absolutely Monte Carlo detector efficiency obtained for Co-60 radionuclide for organ small intestine content with the Ludlum 44-2 placed at the back of abdomen. 53

LIST OF ABBREVIATIONS

ALI	Annual Limit on Intake
AMAD	Activity Median Aerodynamic Diameter
CDC	Center of Dieses Control and Prevention
CDG	Clinical Decision Guide
CRCPD	Conference of Radiation Control Program Director
CT	Computed Tomography
ET	Extra Thoracic
GM	Geiger Muller
GUI	Graphical User Interface
GUIDE	Graphical User Interface Design Environment
ICRP	International Commission on Radiological Projection
MCNP	Monte Carlo N-Particle
MCNPX	Monte Carlo N-Particle Extended
NRC	Nuclear Regulatory Commission
NRT	National Response Plant
NURBS	Non-Uniform Rational B-Spline
ORNL	Oak Ridge National Laboratory
PMT	Photo Multiplier Tube
SSW	Surface Source Write
SSR	Surface Source Read
RDD	Radiological Dispersal Device
UFHADM	University of Florida Hybrid Adult Male
UFHADF	University of Florida Hybrid Adult Female

Abstract of Thesis Presented to the Graduate School
of the University of Florida in Partial Fulfillment of the
Requirements for the Degree of Master of Science

SOFTWARE FOR FIRST RESPONDERS ALLOWING FOR INTERPRETATION OF PORTABLE SURVEY METER RESPONSES IN RADIOLOGICAL TRIAGE DECISIONS

By

Badal Juneja

May 2011

Chair: Wesley E. Bolch
Major: Nuclear Engineering Sciences

As the terrorist threat to US remains eminent, training of the first-responder and associated medical emergency staff is a high priority for all governmental agencies. In responding to a terrorist attack in which a radiological dispersal device (RDD) is used, rapid methods of conducting radiological triage of a large number of potentially contaminated individuals are a great challenge. In this study, the use of commercially available portable survey meters is explored for assessing a potential range of effective doses for adult males and females of different body morphometry. I used our reference hybrid pediatric phantoms to obtain data for ICRP 89 reference 1-year, 5-year, 10-year, and 15-year old phantoms. The phantom models were used to simulate children who were internally contaminated with Am-241, Cs-137, Co-60, I-131, and Ir-192 following acute inhalation or ingestion intakes. Monte Carlo radiation transport simulation was used to obtain net count rates corresponding to effective doses of 50, 250, and 500 mSv as a function of time following the exposure for five detector types, two anatomical positions (back of chest and back of abdomen), and four screening distances from the body (0 cm, 30 cm, 100 cm and 200 cm). Measured count rates can be compared to these values to assign one of four possible effective dose ranges. For easy access to

this large dataset, an intuitive graphical user interface in MATLAB was created. This GUI gives first-responders the ability to specify details of an exposure scenario, patient, and detector. The software provides options to display results either as a graph, a table, or simply the effective dose range and corresponding triage condition.

CHAPTER 1
INTRODUCTION

Following the September 11, 2001 terrorist attacks upon the United States, the federal government has been increasingly active in attempts to prevent subsequent assaults on the homeland. However, the terrorist threats toward U.S. continue to exist, thus making training of first-responders and medical emergency staff is a high priority for all government agencies. One of the principal concerns is the use of radioactive substances added to a conventional explosive, such as dynamite, to create a “dirty bomb,” a type of radiological dispersal device (RDD). While an RDD is not as powerful as a nuclear weapon, it remains a threat due to radioactive content dispersal capabilities (Gonzalez 2003, NRC 2007, NCRP 2010). The spread of radioactivity rages only a few blocks or miles from the origin of the explosion, as opposed to hundreds of miles in case of a nuclear bomb (NRC 2007). Even with this limited spread, a dirty bomb can be a serious concern in an urban environment, or if used in a subterranean metropolitan train system, it could paralyze a city due to widespread panic and workflow disruption (Gonzalez 2003). The extent of local contamination depends on size of the explosive, the amount and type of radioactive material used, and the means of dispersal and weather conditions (NRC 2007).

The abundance of radioactive sources that can be used in an RDD is detailed in by the NCRP (2010) and Gonzalez (2003). Radioactive sources, such as Co-60 and Cs-137) are widely used in medical, industrial, agricultural, and research applications. The source security has been in place to prevent accidental access or petty theft, and there are no sophisticated antiterrorist security measures even on a regulated source (Gonzalez 2003). These radionuclides can be stolen and diverted with relative ease, so

an RDD remains an eminent threat that requires dedicated guidelines for potential terrorist event. However, The NCRP also discusses that it is improbable to get large enough quantity of Pu-238 and Pu-239 for RDDs due to high security and the lack of use in routing commerce and industry (NCRP 2010).

The Government agencies have developed emergency response plans for such events at the federal, state, and local levels (NRT 2004). In an RDD event, the explosion is expected to cause more harm than the radioactive material. The concerns after such an event include the terror and psychological trauma, contaminated property, and the potentially costly cleanup that will follow the explosion (NRC 2007). The existing legal frameworks that could apply to RDD cleanups, concerns raised by the application of such frameworks, and options for mitigating those concerns are details by Elcock et. al. (2004). According to Maiello and Groves, a radiological emergency response starts with measuring and tracking radioactivity in the affected environment, including computer modeling in the early stages of the emergency followed by securing and remediating the affected area and as necessary treating affected personnel (Maiello and Groves 2006).

However, there are additional concerns involved with treating affected personnel. The first is the large number of individuals concerned about their safety and the safety of their loved ones. According to the U.S. Nuclear Regulatory Commission (NRC), a dirty bomb is not a “Weapon of Mass Destruction” but a “Weapon of Mass Disruption,” where contamination and anxiety are the terrorists’ major objective (NRC 2007). After such an event, thousands of individuals need to be examined for internal contamination to assess their treatment needs. While most people will have little to no contamination,

some individuals with high contamination will require immediate attention. The Radiation Studies Branch of the Centers for Disease Control and Prevention (CDC) have posted guidance on the use of nuclear medicine gamma-cameras as make-shift whole-body counters to handle these types of large events. However, it is difficult to transport potentially unmanageable numbers of individuals to specialized nuclear facilities with whole-body counters. The second key issue with treating affected personnel is the safety and protection of the healthcare providers from radiation emitted by the contaminated individuals. After an RDD event, with mass casualties, healthcare providers must make rapid decisions. However, there can be an unduly delay by a decontamination process that may be unnecessary for protecting the health and safety of the patient or the healthcare provider, especially for those victims who have life-threatening injuries (Smith et al. 2005). In such cases, patients' decontamination needs must be evaluated at the site, as opposed to sending them to a specialized nuclear facility. One of the basic needs for a successful medical response is sufficient and adequate radiation detection equipment for the first responders and medical staff (Maiello and Groves 2006).

In this study, I evaluated the use of a portable survey meter to estimate internal contamination of thousands of potentially contaminated individuals. In June 2006, the CDC Radiation Studies Branch hosted a workshop to discuss potential for such study. One scenario envisioned was the positioning of a shielded (i.e., low background) semi-trailer or other portable facility near the event site through which the individuals would be sent following their external decontamination. After a brief survey meter measurement, a range of potential effective doses can be estimated based on

interpretation of the measured values against those determined by Biokinetic modeling and Monte Carlo phantom simulations of the detector response using various phantoms. The influence of the low background count rate can then be reduced by subtracting the background count rate from the radiation detector reading for a contaminated individual. The need for this study was emphasized in the NCRP report on management of persons contaminated with radionuclides (NCRP 2008).

The external contamination can be reduced significantly, as much as 90%, by simply removing the clothing of an effected individuals (Smith et al. 2005). If the victim was sparsely dressed; however, the reduction in external contamination will be less than 90%. The details on how to decontaminate an individual are outlined in greater detail by the NCRP (2008) and CRCPD (Conference of Radiation Control Program Directors) (2006). The clothing should be removed without pulling it over the head to avoid the outer layer from coming in contact with the nose and mouth area. The clothing should be double bagged whenever possible and sealed to prevent the spread of contamination. Decontamination of skin can be achieved simply by gentle washing with soap and lukewarm water followed by a thorough water rinse. The eyes should be flushed with plenty of water. After such an extensive external decontamination process, most individuals will be virtually free of all the external contamination, yet the little residual external contamination will affect the estimated internal contamination. However, this will only change the triage condition in extreme cases, and, in such cases, it will give the more conservative estimates.

The use of a portable survey meter to assess the internal contamination of an individual has not been studied with great detail. A variant of this approach was

considered by CRCPD in their Handbook for Responding to a Radiological Dispersal Device (CRCPD 2006). The handbook notes that when a large population must be surveyed, it is acceptable to perform only a screening survey with survey meter probe 1 to 2 inches away from the body. The Handbook further suggests if nasal area contamination exceeds 100,000 cpm using a Pancake GM probe, a nasal swab or nasal blow can be used to estimate inhaled radioactivity from nasal contamination.

For this study, I used hybrid phantoms, described in detail by Lee et al. (2010) and Johnson et al. (2009), to create photon fluence maps at the posterior surface of an internally contaminated individual for five different radionuclides of interest and all relevant source tissues. As discussed by Johnson et al., to better estimate internal contamination of the diverse US population, six adult and five pediatric phantoms were utilized from their study (Johnson et al. 2009). These photon fluence maps were then used to determine the detector count efficiencies in one GM-based and four NaI-based survey meters at various anatomical positions and measurement distances. These data were then utilized to estimate time-dependent detector count rate thresholds corresponding to 50, 250, and 500 mSv of effective dose. The 50 and 500 mSv values correspond to 1 and 10 Annual Limits on Intake (ALI) that have been used by CDC. These values are based upon ICRP 30 models and current NRC regulations for Bq values of 1 ALI. The 250 mSv values correspond to 5 ALI and is introduced in NCRP Report 161 as a Clinical Decision Guide (CDG) (NCRP 2008). The results were imported into software with intuitive Graphical User Interface (GUI) for easy access to the data.

CHAPTER 2
MATERIALS AND METHODS

Hybrid Patient-Dependent Phantoms Representing Internally Contaminated Individuals

In this study, six adult and five pediatric hybrid computational phantoms were used to represent individuals, of different age and gender, internally contaminated following an acute inhalation or ingestion exposure. To better sample the diverse US population, in addition to 50th weight and height percentile adult male and female phantoms, the 10th and 90th weight percentile phantoms were chosen for both genders at 50th height percentile (Table 2-1). These six adult phantoms (Figure 2-1) were obtained from the Hybrid Patient-Dependent series for U.S. adult population(Johnson et al. 2009). As outlined by the authors, in order to create patient-dependent adult male and female phantoms, the UF hybrid adult male (UFHADM) and the UF hybrid adult female (UFHADF) phantoms, respectively, were modified according to the target parameters, such as weight, standing height, sitting height, arm circumference, waist circumference among others. The UFHADM was created using CT imaging data (330 CT images at 3-mm slice thickness and 512 x 512 matrix size) of a 36-year Korean male volunteer, and UFHADF was created using CT imaging data (258 CT images at 4.5-mm slice thickness and 512 x 512 matrix size) of a 24-year female patient. Major organs were segmented within the CT images. The phantoms are represented as a series of polygon mesh and NURBS (non-uniform rational B-spline) surfaces, and can be imported into Monte Carlo based software, such as MCNP (Pelowitz 2005), by converting them to a binary format.

Five pediatric hybrid computational phantoms (Figure 2-2) were used in this study: gender-neutral 1-year, 5-year, and 10-year old phantoms and gender-specific 15-year-old phantoms. It was assumed that up to age 10, the gender-specific differences in

organ positions and shape other than sex organs were not fully developed (ICRP 2002). The five hybrid pediatric patients were obtained from Lee et al (2010) to be at the same height and weight as the ICRP 89 reference pediatric phantoms (Table 2-1). The 1-year-old phantom was based on a 2-year-old female head CT data and a 1-year-old female torso CT data. The 5-year-old and 10-year-old phantoms were created using, respectively, 4-year-old female CT data for both the head and torso and a 12-year-old male head CT with an 11-year-old male torso CT data. The 15-year-old male phantom was based on a downscaled 18-year-old male head CT data and a 14-year-old male torso CT data. The 15-year-old female phantom was created by using head CT data of 15-year-old female and torso CT data of a 14-year-old female.

These phantoms were then converted from their polygon mesh and NURBS form to voxelized form more suited for use in the Monte Carlo transport code MCNPX (Pelowitz 2005) using an in-house MATLAB code Voxelizer 6.0. While the 1-year-old phantom was voxelized at 1.5 mm x 1.5 mm x 1.5 mm, the older phantoms were voxelized at coarser resolution: 2 mm x 2 mm x 2 mm for the 5-year-old phantom; 2.5 mm x 2.5 mm x 2.5 mm for the 10-year-old phantom; 3 mm x 3 mm x 3mm for the 15-year-old as well as all the adult phantoms. The coarser resolutions for larger phantoms were chosen to increase the computational efficiency in the Monte Carlo simulation of detector response.

Exposure Scenarios

In this study, 21 exposure scenarios (Table 2-2) were considered based on five radionuclides: Am-241, Co-60, Cs-137, I-131, and Ir-192. These radionuclides were chosen based on their potential use in a radiological dispersal device due to their widespread use and their sufficiently long half-life (DOE/NRC 2003, Sohier and

Hardeman 2006). Only the radionuclides that are strong gamma-emitters were considered, so Sr-90 was not part of this study. For each radionuclide, one ingestion and multiple inhalation scenarios were considered based on particle size (1 or 5 μm AMAD) and solubility class (type S, M, or F). However, for each radionuclide, only those combinations of particle size and solubility class were considered for which effective dose coefficient (Sv per Bq-intake) were provided in ICRP Publication 72 (ICRP 1995). Thus, as seen in Table 2-2, while for Am-241 only one solubility class (type M) was considered with both particle sizes (1 and 5 μm AMAD), for Ir-192 all three solubility classes were considered for both particle sizes.

Derivation of Detector Response Functions and Count Rate Thresholds

One of the major goals of this study was to develop an equation that relates the estimate of committed effective dose to the measured detector count rate at a certain distance. The effective dose (in Sv) can be estimated (Equation 2-1) as the product of the radionuclide intake I (in Bq) and the ICRP effective dose coefficient e (in Sv/Bq), which for 21 exposure scenarios discussed earlier is summarized in Table 2-2. Since the ICRP effective dose coefficient is larger for Am-241 than any other radionuclide, considerably lower intake of this radionuclide will give the same effective dose estimate as the other four radionuclides.

$$E\ (Sv) = [I(Bq_{intake})]\left[e\left(\frac{Sv}{Bq_{intake}}\right)\right] \quad (2\text{-}1)$$

The radionuclide intake, I, can be estimated as the ratio of the total body activity, $A_{TB}(t)$, and the fractional total body retention of the radionuclide, $f_{TB}(t)$, at time t post intake (Equation 2-2), where $f_{TB}(t) = \sum_s f_s(t)$. These values of $f_s(t)$, defined as the time-dependent fractional amount of the radionuclide intake present in a given source organ

S of the contaminated individual, were taken from the DCAL software provided by the Center for Biokinetic and Dosimetry Research at the Oak Ridge National Laboratory (ordose.ornl.gov).

$$I(Bq_{intake}) = \frac{[A_{TB}(t)(Bq_{TB})]}{\left[f_{TB}(t)\left(\frac{Bq_{TB}}{Bq_{intake}}\right)\right]} \quad (2\text{-}2)$$

The total body activity, $A_{TB}(t)$, can be approximated at a distance *x* from the individual as shown in Equation 2-3. In the equation the detector net count rate $r_D^x(t)$ (in count per second – cps) is assessed at position *x* at time *t* post-intake. The absolute detector efficiency, $\epsilon_D^x(t)$, is the counts registered per emitted photon from the body at position x, time t post-intake, and Y_{total} is the total yield of x-ray and gamma-ray photons emitted by the radionuclide (photons per second per Bq in body).

$$A_{TB}^x(t)(Bq_{TB}) = \frac{[r_D^x(t)(cps)]}{\left[\epsilon_D^x\left(\frac{cps}{\frac{\gamma_{TB}}{s}}\right)\right]\left[Y_{total}\left(\frac{\frac{\gamma_{TB}}{s}}{Bq_{TB}}\right)\right]} \quad (2\text{-}3)$$

The absolute detector efficiency, $\epsilon_D^x(t)$, gets contributions from multiple contaminated organs, so the $\epsilon_D^x(t)$ can be calculated (Equation 2-4) by summing, over all contaminated source organs, the product of $\epsilon_{MC,S}^x$, the number of registered detector counts at position x per simulated photon emitted from source organ S, and $f_S^{Norm}(t)$, the normalized fraction of total body activity in source organ S at time t post intake.

$$\epsilon_D^x\left(\frac{cps}{\frac{\gamma_{TB}}{s}}\right) = \sum_s[\epsilon_{MC,S}^x\left(\frac{c}{\gamma_s}\right)]\ \left[f_s^{Norm}(t)\left(\frac{\gamma_s}{\gamma_{TB}}\right)\right] \quad (2\text{-}4)$$

As given in Equation 2-4, the detector absolute efficiency for the radionuclide at time t post intake is a weighted average of its values for individual source organs within the phantom. These time independent values need to be assessed only once for a given phantom, source organ, detector type, and position. The other known parameter

from Equation 2-3, the total yield of the emitted photons per unit activity, is simply the summation of the energy-dependent photon yields across the energy spectrum of x-ray and gamma-ray (Equation 2-5). The full photon spectra were sampled for each simulation using the energies and yields given in the data tables of Eckerman and Endo (2008) for each of the 5 radionuclides. Only the energies with yields greater than 0.1% were considered.

$$Y_{total}\left(\frac{\frac{\gamma_{TB}}{s}}{Bq_{TB}}\right) = \sum_i Y_i\left(\frac{\gamma_i}{transformation}\right) \tag{2-5}$$

Combining Equation 2-1 through 2-5 gives the final expression (Equation 2-6) for estimating the contaminated individual's committed effective dose following an acute inhalation or ingestions.

$$E(Sv) = \frac{[r_D^x(t)(cps)]\left[e\left(\frac{Sv}{Bq_{intake}}\right)\right]}{\left\{\sum_s\left[\varepsilon_{MC,S}^x\left(\frac{C}{\gamma_S}\right)\right]\left[f_s^{Norm}(t)\left(\frac{\gamma_S}{\gamma_{TB}}\right)\right]\right\}\left[\sum_i Y_i\left(\frac{\frac{\gamma_{TB}}{S}}{Bq_{TB}}\right)\right]\left[f_{TB}(t)\left(\frac{Bq_{TB}}{Bq_{intake}}\right)\right]} \tag{2-6}$$

This final expression can be collapsed (Equation 2-7) to express effective dose as product of net detector count rate (in cps or cpm) and a time-dependent effective dose response function $R_E^x(t)$.

$$E(Sv) = [r_D^x(t)(cps)]\left[R_E^x\left(\frac{Sv}{cps}\right)\right] \quad or \tag{2-7}$$

$$E(mSv) = [r_D^x(t)(cpm)]\left[R_E^x\left(\frac{mSv}{cpm}\right)\right]$$

Now, if a specific value of threshold effective dose, E_{Thres}, is assumed, the time-dependent net count rate thresholds r_{thres}^x can be calculated using Equation 2-8.

$$r_{Thres}^x(t)(cpm) = \frac{E_{Thres}(mSv)}{R_E^x\left(\frac{mSv}{cpm}\right)} \tag{2-8}$$

Three threshold effective doses, 50 mSv, 250 mSv, and 500 mSv were chosen for this study. Based on these three threshold effective doses, four triage decisions can be evaluated: below 50 mSv, between 50 and 250 mSv, between 250 and 500 mSv, and exceeding 500 mSv.

Phantom Source Regions

In this study, 50 different combinations of radionuclide and source organs were considered. These combinations are summarized in Table 2-3. The dots in the table correspond to the source organs for which Monte Carlo transport was explicitly performed. The source organs with squares never exceeded 1% of intake activity, and were lumped in the larger “other tissues” category. This category was modeled in the phantoms as the collection of all soft tissues for which an explicit value of $f_s(t)$ was not already specified. For the blood source, Table 2.14 of ICRP publication 89 (ICRP 2002) was consulted. A collapsed version of this table was implemented, as many of the tissues have reference values less than 1% of total blood volume. Total blood volume was thus modeled using 12 source regions, with the same percent distribution for both genders, as shown in Table 2-4.

Organ Source Definition

As described in the MCNP manual (Booth et al. 2003), for repeated structures (such as lattices used to import voxel phantoms), instead of specifying a cell, a cell path can be specified that maps the detail of the cell and the lattice cell structure in which the cell resides. For example, cell path (11<999<1000) refers to cell 11 in the lattice specified by cell 999 that is used to fill cell 1000. Although this method will accurately sample the desired organ, it is a highly inefficient method. When organs are specified in this manner, MCNP samples a random voxel in the entire lattice, yet only accepts it as

source if it is placed in the voxel specified by cell 11. This becomes inefficient as voxel tag 11 (ET1 in our case) is only a small part (the volume of this region is 0.0053% of the total volume) of body, which means 99.9947% of the source point generated will be discarded. An alternative method is to use the same cell path structure with a more specific lattice position for the source generation. For example, the cell path (11<999[57 12 128]<1000) will sample only in the element in the lattice specified by the indices specified in the square bracket. While highly efficient, this method is difficult to implement as there are 100s of voxels corresponding to ET1 in the phantom. In the case of residual soft tissue, this number increases to a few million. All these individual elements of the lattice need to be specified to sample the organ correctly. A visual basic code was written to generate the necessary input for all the organs of interest automatically rather than doing this manually. Once the new source definitions were put in place, tenfold speed increase was noticed in most cases.

SSW/SSR

To further optimize the computation efficiency a method known as surface source write (SSW) explained in the MCNPX manual was considered (Pelowitz 2005). This method uses any geometry (in our case a rectangular surface) to record energies and directions of the particles crossing that surface. This new surface can then be used as a source for subsequent runs, using the Surface source read (SSR) card, for different detector models (described later) and distances. To get an accurate distribution of photon behavior on the surface-source, more particle histories than regular are necessary. For this study, I simulated 100 million particles for each organ and radionuclide combination. Roughly 75% of these particles were recorded on the surface-source. As necessary, in house codes were written using MATLAB to automate

cumbersome tasks of generating and retrieving data from 550 inputs necessary generate SSW files (50 radionuclide-organ combinations for 11 phantoms) and close to 10,000 output files (for 17 detector input files described later for each of 550 SSW).

Monte Carlo Detector Models

Five detectors were investigated in this study: (A) the Ludlum 44-9 GM probe, (B) the Ludlum 12S survey meter, (C) the Capintec Captus 3000 thyroid probe, (D) the Ludlum 44-2 survey probe, and (E) the Canberra InSpector 1000 survey meter. All the detectors have a NaI scintillator except the Ludlum 44-9 GM probe. While the MCNPX models for the 12S survey meter was created at the University of Florida, the other four detector models were obtained either from Dr. Hertel's group at Georgia Institute of Technology or the manufactures. The MCNPX models were constructed using both physical measurements of the actual device and schematic diagrams provided by the manufacturers. MCNPX's F8 (pulse-height distribution tally) was used to find the detectable pulses in the detector's sensitive volume. For the four detectors with a NaI scintillator it was assumed that an event with an energy deposition less than 30 keV will not contribute. For the GM probe, an energy cut-off of 1.58 keV was applied.

The model for the Ludlum 44-9 GM probe is shown in Figure 2-3A. For this model, the wire mesh covering and mica window were modeled, along with the probe handle. The sensitive volume was filled with a gas composed of 92, 7.5, and 0.5 atom percent of Neon, Argon, and Bromine, respectively. Figure 2-3B displays the MCNPX model for the Ludlum 44-2 survey probe with a 1 inch x 1 inch NaI crystal scintillator. The NaI crystal is encased in aluminum housing. The housing is situated inside an aluminum detector case that also incorporates the photo multiplier tube (PMT) and form factor. The MCNPX model of Canberra InSpector 1000 is shown in Figure 2-3C. This model

has a 2 inch x 2 inch NaI crystal encased in an aluminum cylinder. The PMT was also modeled for this detector. Figure 2-3D displays the Ludlum 12S survey meter. The computational model for this detector has a 1 inch x 1 inch NaI crystal inside an aluminum housing that is situated within an aluminum casing. The aluminum casing also houses a battery case and two circuit boards. The remainder of the detector was considered to be air-filled at a standard pressure and temperature. The MCNPX model of Capintec Captus 3000 thyroid probe is shown in Figure 2-3E. The detector was modeled with a sensitive NaI volume, aluminum casing, and lead innards.

These detector models were used with previously generated SSW/SSR files for all 11 phantoms. For each detector model, except the Ludlum 44-9 GM probe, two separate instances of the detector were placed 0 cm, 30 cm, 100 cm, and 200 cm away from the back of the phantom (now represented by the SSW files) at two different anatomical positions: back of chest and back of abdomen. Since the Ludlum 44-9 GM probe is a very inefficient detector, it was only simulated at contact with the phantoms to get meaningful results. In the end, a total of four sequential Monte Carlo simulations (one at each distance) were performed for each of the eleven phantoms, each source organ and radionuclide combination, and from every Monte Carlo simulation two values of $\epsilon_{MC,S}^{x}$ (chest and abdomen) and corresponding relative statistical errors were extracted using a MATLAB code.

The average of relative statistical errors, on values of $\varepsilon_{MC,S}^{x}$, over eleven phantoms, fifty radionuclide and source organ combinations, five detectors, and four distances was 1.42%. For the most parts, the errors were significantly lower, but the higher average is the result of Am-241 detector simulation at the distances of 100 and 200 cm from the

phantom. As Am-241 yields very low-energy gamma rays, which were mostly absorbed in the phantom body during the Monte Carlo simulation, we recommend when assessing triage condition greater distances should be used cautiously with Am-241. The data was obtained in this study for completeness. About 2% of total statistical errors were greater than 10%, all corresponding to Am-241 at 100 or 200 cm distance. The statistical errors were ~1% for distances of 0 and 30 cm and ~3% for 100 cm distance.

Creating a Graphical User Interface

To assist with triage decisions a Graphical User Interface (GUI) was created using MATLAB, which was chosen to be the programming language of interest due to an exceptionally efficient handling of large matrices that store the results of Monte Carlo simulations. The GUI was designed using Graphical User Interface Design Environment (GUIDE), a utility provided as part of the MATLAB package. The actions corresponding to the buttons were then added to the preliminary code generated by GUIDE. The GUI has capabilities to display the results in both graphical and tabular format based on the information regarding the individual (age, gender, and weight percentile), exposure scenario, and examination protocol (detector, distance, and anatomical position). The tabular results can also be exported to an Excel sheet. The triage condition can then be assessed if the background radiation count rate, detector output for the individual and time since exposure are provided. If the detector count rate exceeds the detector saturation count rate (875,000 cpm for NaI detectors and 100,000 cpm for the GM probe), the GUI will show a warning message and will not asses the triage condition.

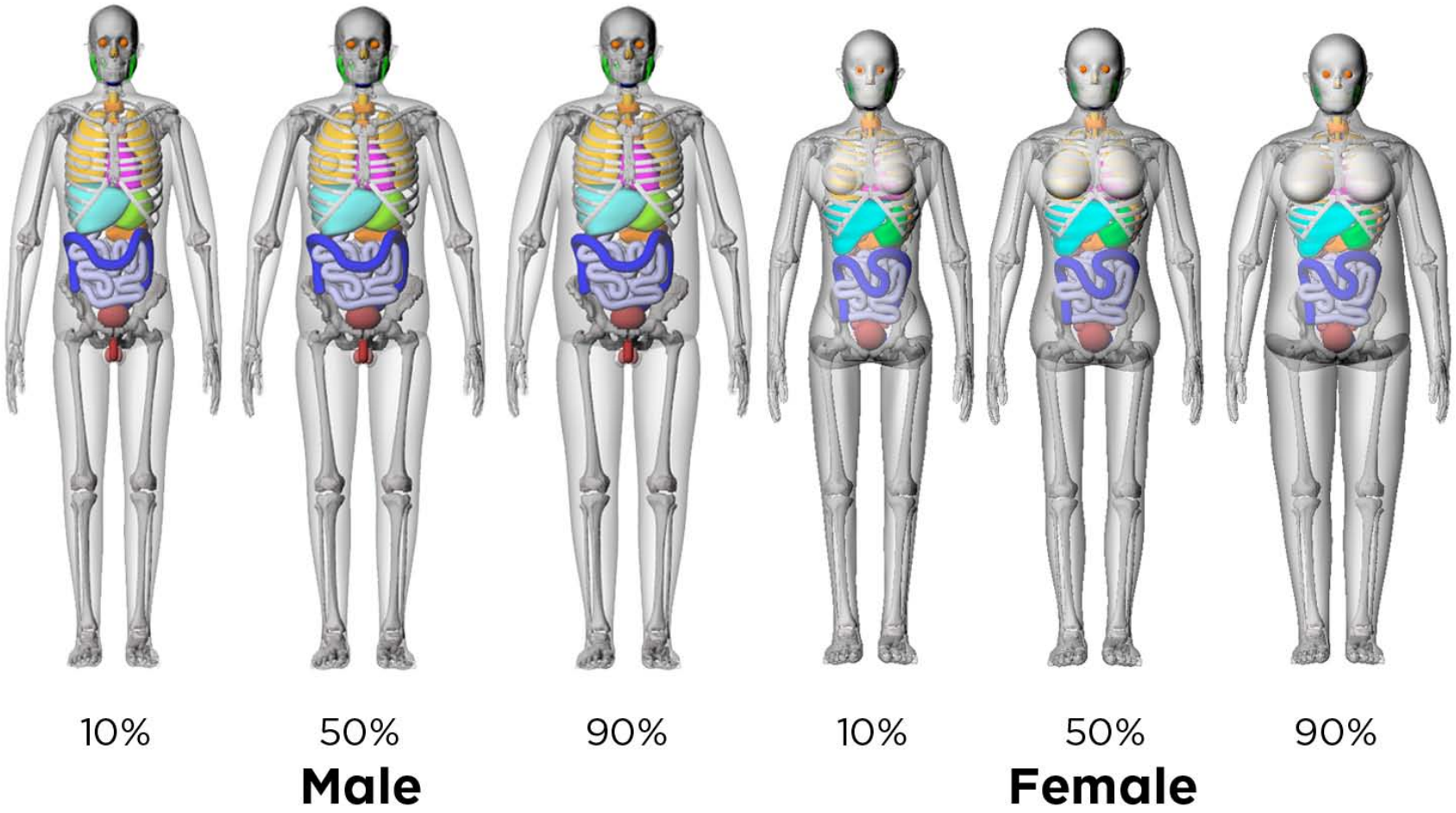

Figure 2-1. The University of Florida's Hybrid Computational Phantoms representing (from left to right) 10th, 50th, and 90th weight percentile adult male and 10th, 50th, and 90th weight percentile adult female.

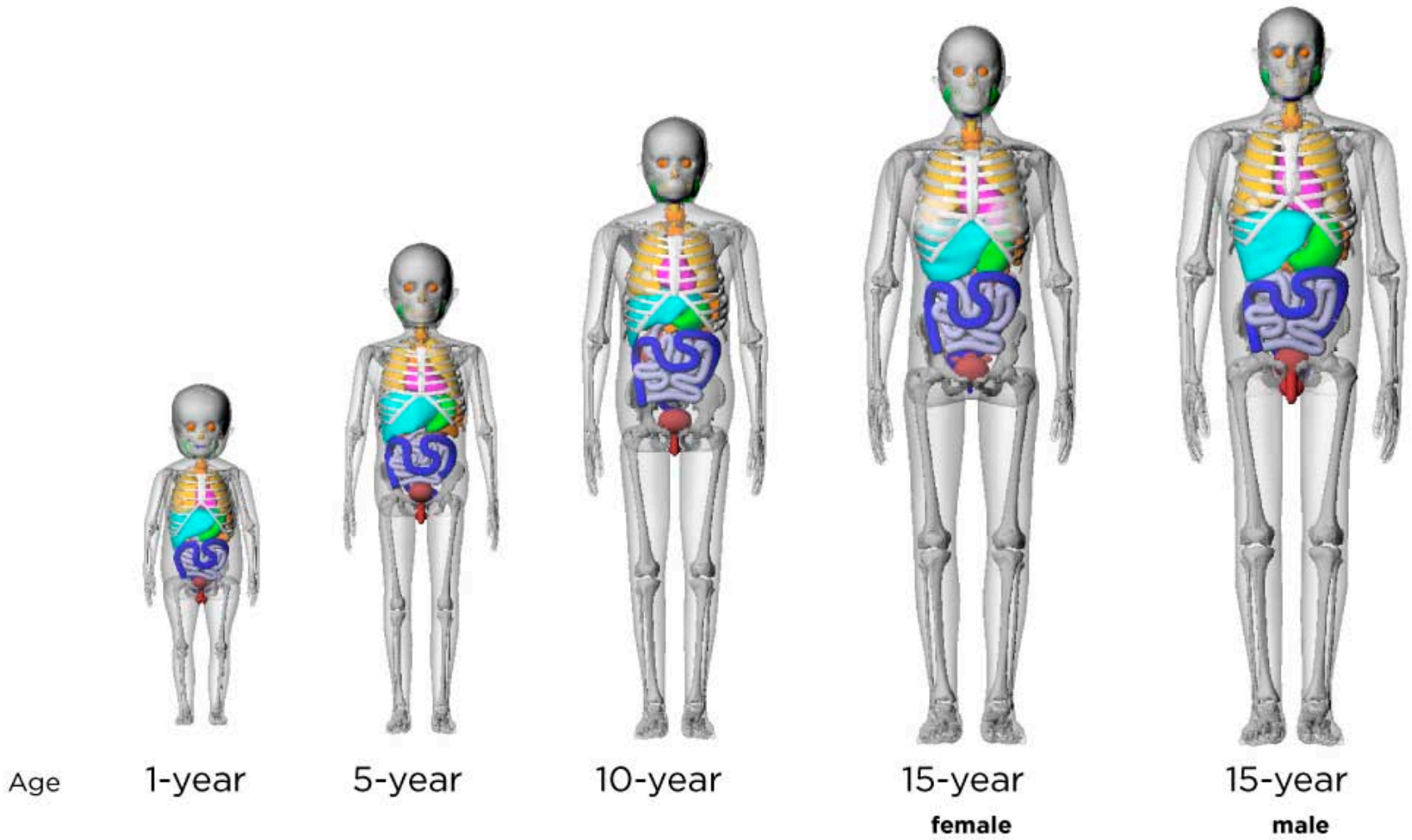

Figure 2-2. The University of Florida's Hybrid Computational Phantoms representing (from left to right) 1-year, 5-year, 10-year, 15-year (female) and 15-year (male) 50th weight percentile individuals

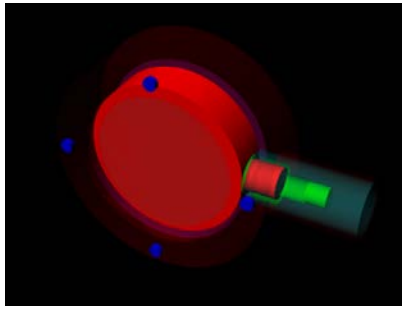

(A)

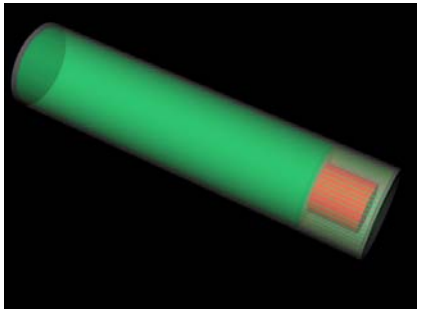

(B)

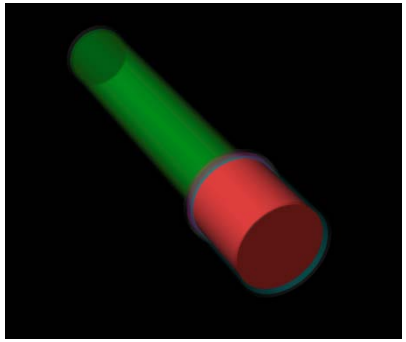

(C)

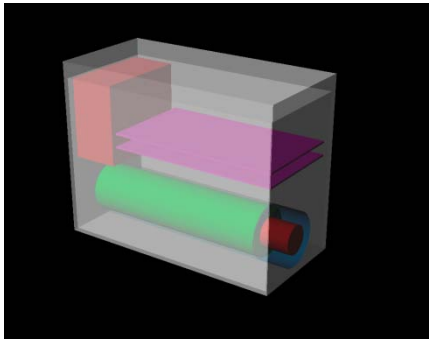

(D)

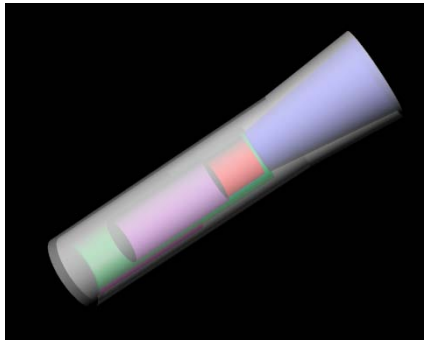

(E)

Figure 2-3. Rhinoceros models of the five detectors used in this study: A) Ludlum 44-9 GM Probe, B) Ludlum 44-2 Survey Meter, C) Canberra InSpector 1000 Survey Meter, D) Ludlum 12s Survey Meter, and E) Capintec Captus 3000.

Table 2-1. Height and Weight of the eleven phantoms used in this study

Phantoms			
Age/Gender	**Weight %**	**Standing Height (cm)**	**Weight (kg)**
1-year-old		76	10.3
5-year-old		109	18.0
10-year-old		138	33.6
15-year-old Male		167	58.3
15-year-old Female		161	55.0
Adult Male	10	173	64.1
	50	173	78.4
	90	173	97.3
Adult Female	10	160	51.7
	50	160	66.8
	90	160	90.4

Table 2-2. Summary of dose coefficient for Effective Dose (Sv per Bq intake) for all 21 exposure scenarios considered in this study for different age groups.

Exposure Scenario	Radionuclide	Intake	AMAD	Solubility Class	Effective Dose				
					Adult	1 year	5 year	10 year	15 year
1	Am-241	Inhal	1 μm	Type M	4.20E-05	6.90E-05	5.10E-05	4.00E-05	4.00E-05
2	Am-242	Inhal	5 μm	Type M	3.10E-05	3.70E-05	3.30E-05	2.70E-05	3.20E-05
3	Am-243	Inges			2.00E-07	3.70E-07	2.70E-07	2.20E-07	2.00E-07
4	Co-60	Inhal	1 μm	Type M	1.00E-08	3.40E-08	2.10E-08	1.50E-08	1.20E-08
5	Co-61	Inhal	1 μm	Type S	3.10E-08	8.60E-08	5.90E-08	4.00E-08	3.40E-08
6	Co-62	Inhal	5 μm	Type M	8.00E-09	2.30E-08	1.70E-08	1.20E-08	1.00E-08
7	Co-63	Inhal	5 μm	Type S	1.90E-08	4.20E-08	3.60E-08	2.20E-08	2.30E-08
8	Co-64	Inges			3.40E-09	2.70E-08	1.70E-08	1.10E-08	7.90E-09
9	Cs-137	Inhal	1 μm	Type F	4.60E-09	5.40E-09	3.60E-09	3.70E-09	4.40E-09
10	Cs-138	Inhal	5 μm	Type F	6.70E-09	6.80E-09	5.10E-09	5.10E-09	6.80E-09
11	Cs-139	Inges			1.30E-08	1.20E-08	9.60E-09	1.00E-08	1.30E-08
12	I-131	Inhal	1 μm	Type F	7.40E-09	7.20E-08	3.70E-08	1.90E-08	1.10E-08
13	I-132	Inhal	5 μm	Type F	1.10E-08	8.60E-08	5.00E-08	2.50E-08	1.70E-08
14	I-133	Inges			2.20E-08	1.80E-07	1.00E-07	5.20E-08	3.40E-08
15	Ir-192	Inhal	1 μm	Type F	1.80E-09	1.10E-08	5.70E-09	3.30E-09	2.10E-09
16	Ir-193	Inhal	1 μm	Type M	5.20E-09	1.80E-08	1.10E-08	7.60E-09	6.40E-09
17	Ir-194	Inhal	1 μm	Type S	6.60E-09	2.20E-08	1.30E-08	9.50E-09	8.10E-09
18	Ir-195	Inhal	5 μm	Type F	2.20E-09	1.20E-08	6.90E-09	4.00E-09	2.80E-09
19	Ir-196	Inhal	5 μm	Type M	4.50E-09	1.30E-08	8.00E-09	5.90E-09	6.30E-09
20	Ir-197	Inhal	5 μm	Type S	5.50E-09	1.50E-08	9.40E-09	7.00E-09	7.60E-09
21	Ir-198	Inges			1.40E-09	8.70E-09	4.60E-09	2.80E-09	1.70E-09

Table 2-3. Source Organs and tissue modeled in the computational phantoms for each of the five radionuclides considered in this study. Organs for which the fractional uptake never exceeds 1% were not considered in modeling survey meter response functions.

Souce Tissue	Am-241	Co-60	Cs-137	I-131	Ir-192
ET1	●	●	●	●	●
ET2	●	●	●	●	●
Trachea & Lungs	●	●	●	●	●
Stomach Contents	●	●	●	●	●
Small Intestine Content	●	●	●	●	●
Blood	●	●	●	●	●
Left Colon Content	●	●	●	●	●
Right Colon Content	●	●	●	●	●
Liver	●	●			●
Other Tissues	●	●	●	●	●
Skeleton	●				
Kidneys	■				■
Testes	■				
Ovaries	■				
Thyroid				●	
Spleen					■
Urinary Bladder	■	■	■	■	■

Note: Other Tissues are defined as all soft tissues of the phantoms excludes those listed above.

Note: Squares indicate tissues with uptake fractions never exceeding 1%

Table 2-4. Selection of source tissues and organs in the computational phantoms used to model radionuclide source within circulating blood of the adult male and female.

Blood Sources - ICRP Publication 89			*Blood Sources - Present Study*		
Organ or Tissue	*Male (%)*	*Female (%)*	*Organ or Tissue in Phantom*	*Male (%)*	*Female (%)*
Fat	5.00	8.51	Residual Soft Tissues	46.90	46.90
Brain	1.20	1.20	Brain	1.20	1.20
Stomach / Esophagus	1.00	1.00	Small Intestine Wall	3.80	3.80
Small Intestine	3.80	3.80	Colon	2.20	2.20
Colon	2.20	2.20	Heart Content	9.00	9.00
Right Heart Content	4.50	4.50	Heart Wall	1.00	1.00
Left Heart Content	4.50	4.50	Kidneys	2.00	2.00
Coronary Tissue	1.00	1.00	Liver	10.00	10.00
Kidneys	2.00	2.00	Lungs	12.50	12.50
Liver	10.00	10.00	Skeleton	7.00	7.00
Pulmonary Tissues	10.50	10.50	Skin	3.00	3.00
Bronchial Tissues	2.00	2.00	Spleen	1.40	1.40
Skeletal Muscle	14.00	10.51			
Pancreas	0.60	0.60			
Skeleton					
Red Marrow	4.00	4.00			
Trabecular Bone	1.20	1.20			
Cortical Bone	0.80	0.80			
Other Skeleton	1.00	1.00			
Skin	3.00	3.00			
Spleen	1.40	1.40			
Thyroid	0.06	0.06			
Lymph Nodes	0.20	0.20			
Gonads	0.04	0.02			
Adrenals	0.06	0.06			
Urinary Bladder	0.02	0.02			
All Other Tissues	1.92	1.92			
Aorta and Large Veins	6.00	6.00			
Large Veins	18.00	18.00			
	100.00	100.00		100.00	100.00

CHAPTER 3
RESULTS

Software Output

The Graphical User Interface (Figure 3-1) evaluates count rate thresholds corresponding to 50, 250, and 500 mSv effective doses according to Equation 2-8. The GUI is capable of evaluating these data ranges for all eleven phantoms across the 21 exposure scenarios, five detectors, four screening distances, and two anatomical screening positions. The first two categories of inputs, “Measurement information” and “Patient information,” are required. However, the choice of radionuclide is the only required input from the category “Intake scenario.” If the other input parameters (Exposure, Particle size, and Solubility class) are left untouched, the default values (exposure via inhalation of 1 μm AMAD particle and solubility class type M or F depending on radionuclide) are assumed. If the input parameter “Exposure” is set to Ingestion, the two following input parameters (Particle size and Solubility class) are ignored. The final input category, “Exposure information”, is an optional (yet highly desired) category, and is used to evaluate the triage condition of an individual. The background count rate is the count rate measured with a given detector given the absence of a contaminated individual. This value is subtracted from the gross count rate measured for a contaminated individual to obtain the net count rate produced by internal and leftover external contamination.

Once the input queries are satisfied, the results can be displayed in both graphical and tabular format. A representative graph is displayed in Figure 3-2 for an adult male with 90 weight percentile using Capintec Captus 3000 detector. The detector was placed 100 cm away from the back of the abdomen. Only the radionuclide of interest, Ir-

192, was assumed to be known and the rest of the parameters for intake scenario were left as default (acute inhalation of a 1 μm AMAD aerosol of Type M lung solubility). The same data in the tabular format as exported from the GUI is displayed in Table 5. In Figure 3-2, the three curves correspond to 50 (blue), 250 (green), and 500 (red) mSv effective dose as a function of time extending to 30 days post-intake. The time axis is given on a logarithmic scale where the first decade (0.01 to 0.1 days) corresponds to time scale between ~15 minutes to ~2.5 hours, the second decade (0.1 to 1 day) corresponds to time between ~2.5 hours and 1 day, and remainder of the abscissa extends to 30 days post-exposure.

According to Ludlum Measurement, Inc., the maximum count rate prior to a significant detector saturation and loss of linear response is approximately 875,000 cpm for NaI detectors and 100,000 cpm for the GM pancake probe. The dashed black line in the graph corresponds to these detector saturation values. When a given curve rises above maximum count rate level, those combinations of elapsed time, detector position, and screening distance should be avoided, and another position or distance should be chosen. Figure 3-3a, for example, displays the curves for the Ludlum 44-2 detector placed 30 cm away from the chest of a 50th weight percentile female. The radionuclide of interest was Co-60 and the exposure was known to be due to ingestion. In this case, the curves corresponding to both 250 and 500 mSv effective dose go beyond the detector saturation line. The data from these curves is only useful approximately two days after the exposure. However, if we move 100 cm away from the chest with no other changes in evaluation conditions (Figure 3-3b), curves corresponding to all the threshold effective does are below the saturation line.

The results in the tabular format can also be extracted to a Microsoft Excel worksheet. To assure a unique filename for each Excel worksheet, the filename is automatically generated as a string starting with “Result_” followed by the current date and time. The Excel worksheet not only contains all the data shown in the tabular results, but also the input parameters from the three major input categories: Measurement information, Patient Information, and Intake scenario. A sample Excel worksheet corresponding to the case discussed in Figure 3-2 is attached as Appendix A.

Once the results are obtained in a graphical format, the triage condition can be obtained if three additional parameters are provided: Gross count rate, Background count rate, and Time since exposure. For the adult male case discussed earlier (Figure 3-2), the examination results are shown in Figure 3-4a for the gross count rate of 225,000 cpm and the background count rate of 35,000 cpm one day after the exposure. In this instance, the effective dose is estimated to be between 250 and 500 mSv (Triage Condition III). However, if the gross count rate was 1,000,000 cpm, the result will show an “Exceed Saturation” warning (Figure 3-4b) as the gross count rate is higher than the detector saturation count rate.

Recommendations for Medical Response Based on Estimated Range of Effective Dose

The suggested medical responses based on the estimated range of effective dose are presented in Table 6. Four Radiological Triage Conditions defined in Table 6 corresponds to the estimated effective doses of below 50 mSv (Condition I), between 50 and 250 mSv (Condition II), between 250 and 500 mSv (Condition III), and exceeding 500 mSv (Condition IV). The medical recommendations are given by a letter, which are

explained in footnotes. For example, if the estimated effective dose is less than 50 mSv (Condition I), then the individual should follow-up with primary care physician for routine cancer screening (letter recommendation K). From the table it can also be seen that, if medical evaluation is within 30-60 minutes of the radiation incident, 1) a nasal swabs should be performed to evaluate for inhalation and 2) a gastric lavage should be performed if the effective dose exceeds 50 mSv for an ingestion exposure. If the estimated effective dose is higher 50 mSv, a whole-body counting or nuclear medicine gamma-camera imaging are encouraged to confirm triage conditions (letter recommendation M).

Table 3-1. Representative table for time dependent count rate (in cpm) corresponding to Ir-192 Inhalation (1 micrometer AMAD and Type M solubility class) for the adult male (90th weight percentile) with the Capintec Captus 3000 detector placed 100 cm away from the back of the abdomen.

Time (days)	50 mSv	250 mSv	500 mSv
0.02	5.51E+04	2.76E+05	5.51E+05
0.04	6.18E+04	3.09E+05	6.18E+05
0.08	6.35E+04	3.18E+05	6.35E+05
0.17	6.22E+04	3.11E+05	6.22E+05
0.25	6.05E+04	3.02E+05	6.05E+05
0.33	5.90E+04	2.95E+05	5.90E+05
0.42	5.73E+04	2.87E+05	5.73E+05
0.5	5.56E+04	2.78E+05	5.56E+05
0.58	5.40E+04	2.70E+05	5.40E+05
0.67	5.22E+04	2.61E+05	5.22E+05
0.75	5.05E+04	2.53E+05	5.05E+05
0.83	4.88E+04	2.44E+05	4.88E+05
1	4.51E+04	2.26E+05	4.51E+05
2	2.71E+04	1.36E+05	2.71E+05
3	1.79E+04	8.97E+04	1.79E+05
4	1.40E+04	6.99E+04	1.40E+05
5	1.24E+04	6.19E+04	1.24E+05
6	1.16E+04	5.79E+04	1.16E+05
7	1.12E+04	5.61E+04	1.12E+05
8	1.10E+04	5.48E+04	1.10E+05
9	1.07E+04	5.37E+04	1.07E+05
10	1.06E+04	5.28E+04	1.06E+05
15	9.70E+03	4.85E+04	9.70E+04
20	8.97E+03	4.48E+04	8.97E+04
25	8.31E+03	4.16E+04	8.31E+04
30	7.74E+03	3.87E+04	7.74E+04

Table 3-2. Recommendations for medical response following radiological triage screening by radionuclide and estimated range of effective dose based on survey meter count rate measurements.

	Ranges of Effective Dose and Their Corresponding Recommended Medical Response			
Radionuclide	**Effective Dose** *< 50 mSv* *Triage Condition I*	**Effective Dose** *50 - 250 mSv* *Triage Condition II*	**Effective Dose** *250 - 500 mSv* *Triage Condition III*	**Effective Dose** *> 500 mSv* *Triage Condition IV*
Am-214	**A, K**	**A, B, C, D, F, K, M**	**A, B, C, D, E, F, L, M**	**A, B, C, D, E, F, J, L, M**
Co-60	**A, K**	**A, B, C, D, F, K, M**	**A, B, C, D, E, F, L, M**	**A, B, C, D, E, F, J, L, M**
Cs-137	**A, K**	**A, B, C, D, G, K, M**	**A, B, C, D, E, G, L, M**	**A, B, C, D, E, G, J, L, M**
I-131	**K**	**H, K, M**	**H, L, M**	**H, L, M**
Ir-192	**A, K**	**A, B, C, D, M**	**A, B, C, D, E, I, L, M**	**A, B, C, D, E, I, J, L, M**

Recommendations based on availability of resources:

A If medical evaluation is within 30-60 minutes of the radiation incident,
1. Perform nasal swabs to evaluate for inhalation (see NCRP Report No. 65 or its 2008 revision)
2. If the effective dose exceeds 50 mSv for an ingestion exposure, perform gastric lavage.

B If medical evaluation is within 24 hours of ingestion, provide cathartics

C Obtain baseline Complete Blood Count (CBC), Serum Electrolytes, and Chemistry Panel

D Collect 24-hour urine and stool samples for bioassay analysis

E Obtain serial CBCs every 8 to 12 hours for 3 days, and then daily for an additional 4 days to rule out Acute Radiation Syndrome.

F Prescribe DTPA per FDA guidelines (see FDA website or revision to NCRP Report No. 65). DTPA is FDA approved only for chelation of americium, curium, and plutonium. Other uses of DTPA are off-label. If DTPA will not be available for several hours, consider initiating EDTA treatment per FDA guidelines. EDTA is FDA approved only for lead poisoning. Other uses of EDTA are off-label. Change to DTPA when available.

G Prescribe Prussian Blue (Ferric Ferrocyanate, Radiogardase®) per FDA guidelines (see FDA website or revision to NCRP Report No. 65). Prussian Blue is FDA approved only for cesium and thallium intakes. Other uses are off-label.

H Prescribe potassium iodide (KI) per FDA guidelines. KI is FDA approved only for treatment of radioactive iodine (RAI) intake. Criteria for treatment and dosing is dependent on subject age, and pregnancy and lactation status.

I There is limited clinical experience with the use of Penicillamine (Cuprimine ®) for internal contamination with iridium. Recommend to consider using Penicillamine off-label and follow FDA drug guidance. If Penicillamine is not available, consider using DTPA.

J Consider performing lung lavage for inhalational injury with effective dose > 2000 mSv based on risk/benefit

K Follow-up with primary care physician for routine cancer screening.

L Follow-up with primary care physician for high-risk cancer screening.

M Confirm triage condition (dose range) via (1) whole-body counting or (2) nuclear medicine gamma-camera imaging (see emergency.cdc.gov/radiation)

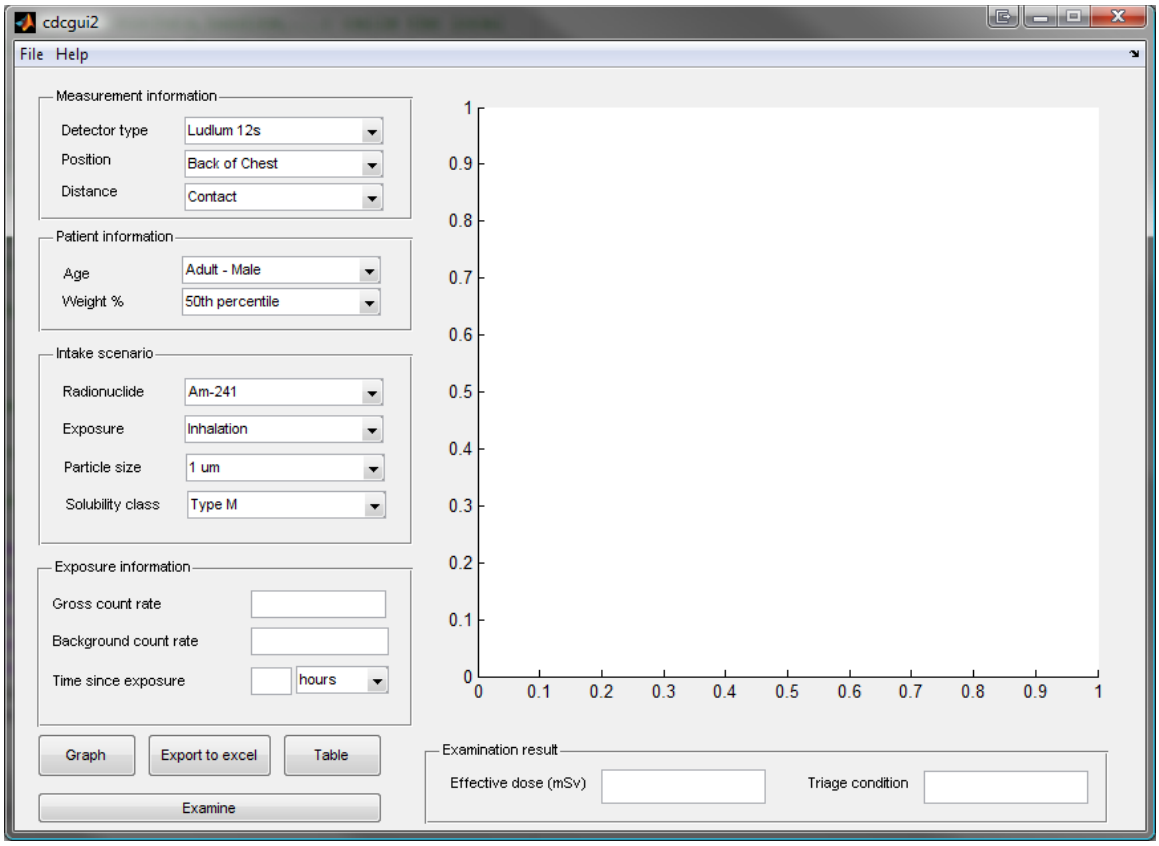

Figure 3-1. The GUI created in MATLAB for easy access to data generated in this study.

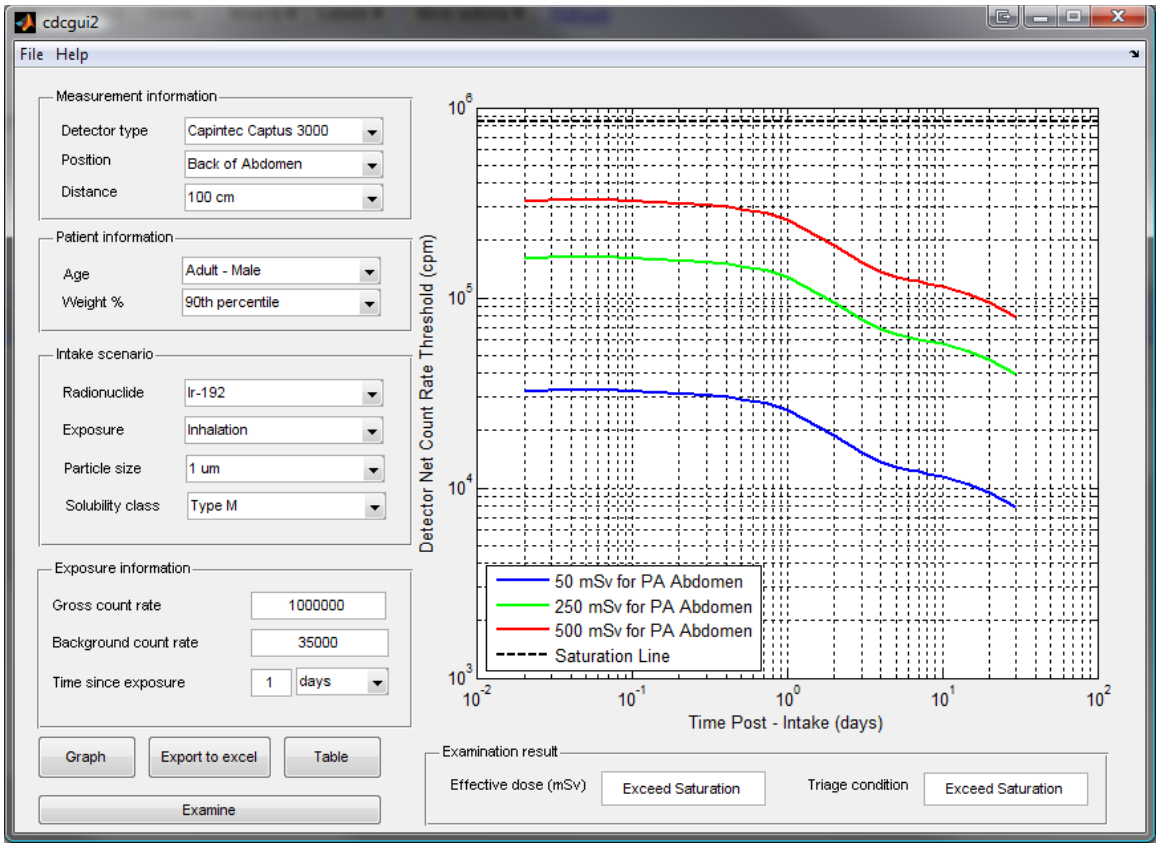

Figure 3-2. Representative graph for time dependent count rate (in cpm) corresponding to Ir-192 Inhalation (1 micrometer AMAD and Type M solubility class) for the adult male (90th weight percentile) with the Capintec Captus 3000 detector placed 100 cm away from the back of the abdomen.

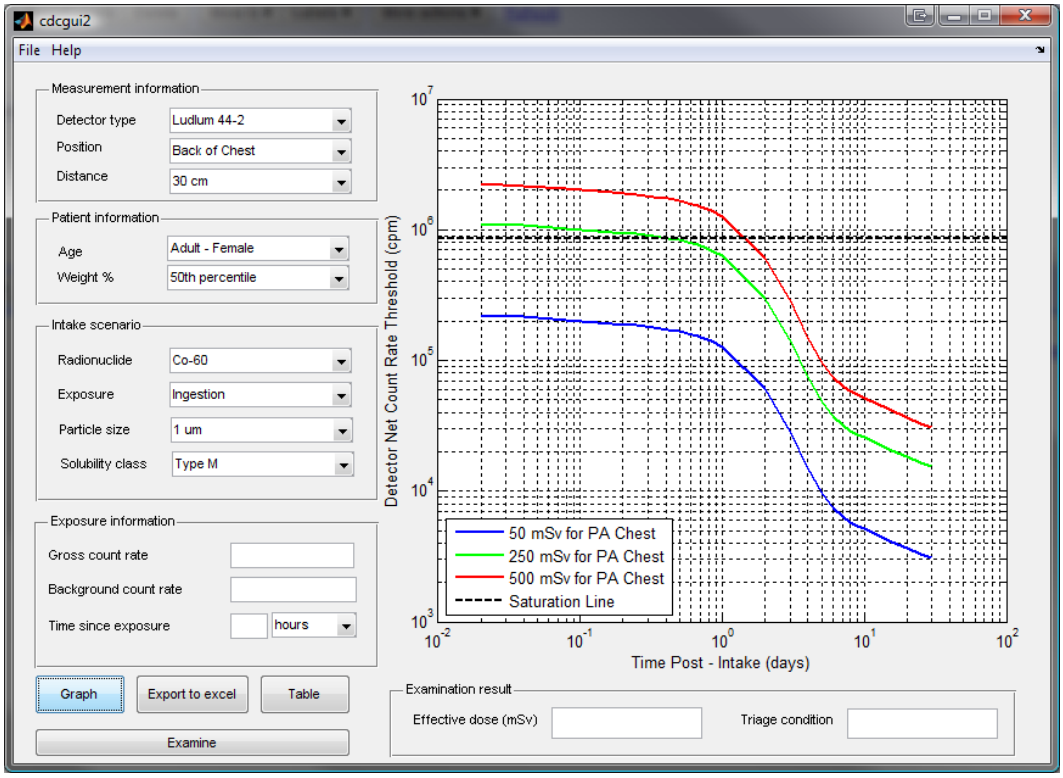

(A)

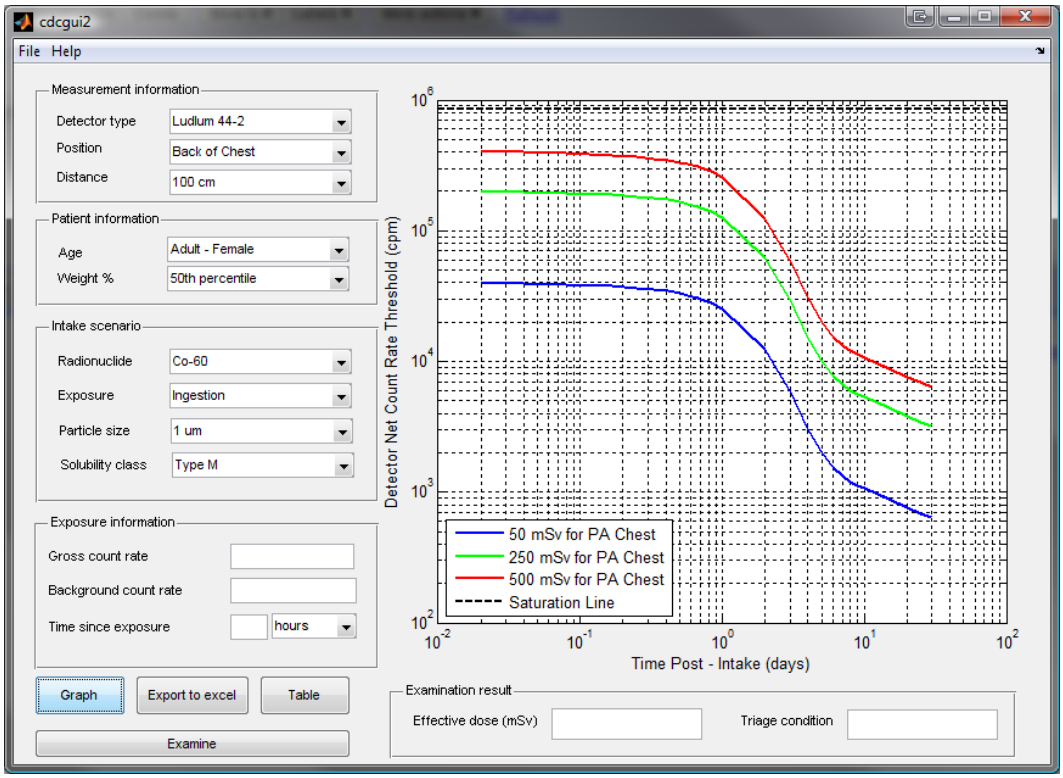

(B)

Figure 3-3. Time dependent count rate (in cpm) corresponding to Co-60 Ingestion for the adult female (90th weight percentile) with the Ludlum 44-2 detector placed (A) 30 cm and (B) 100 cm away from the back of the chest.

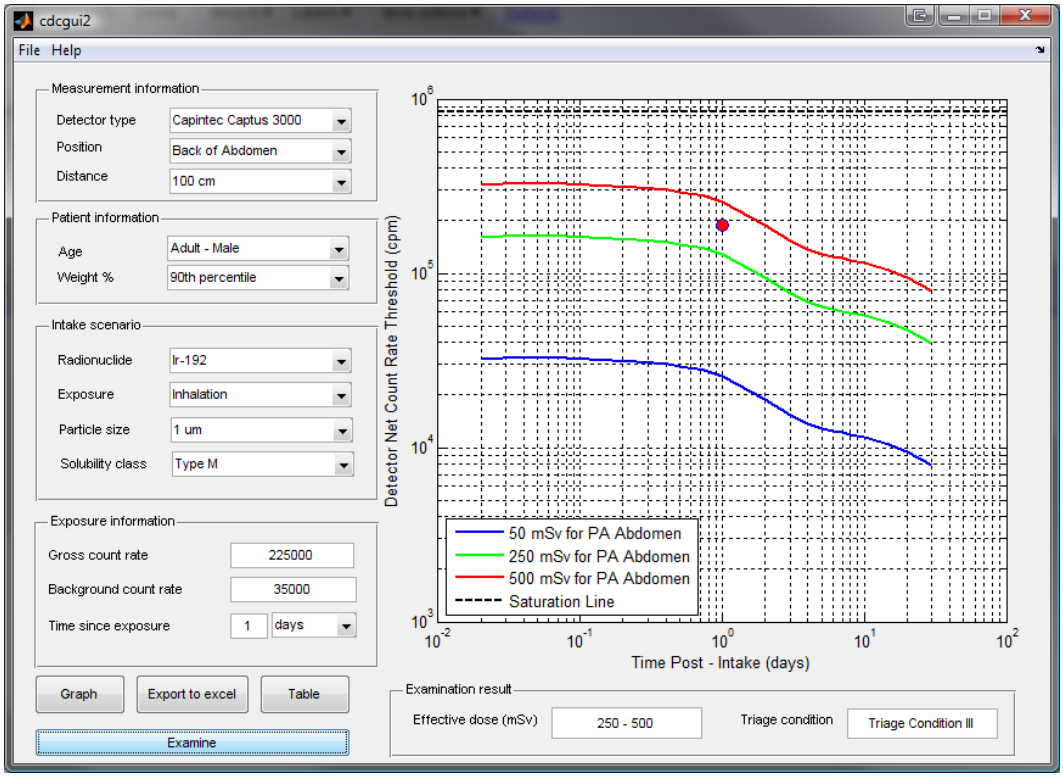

(A)

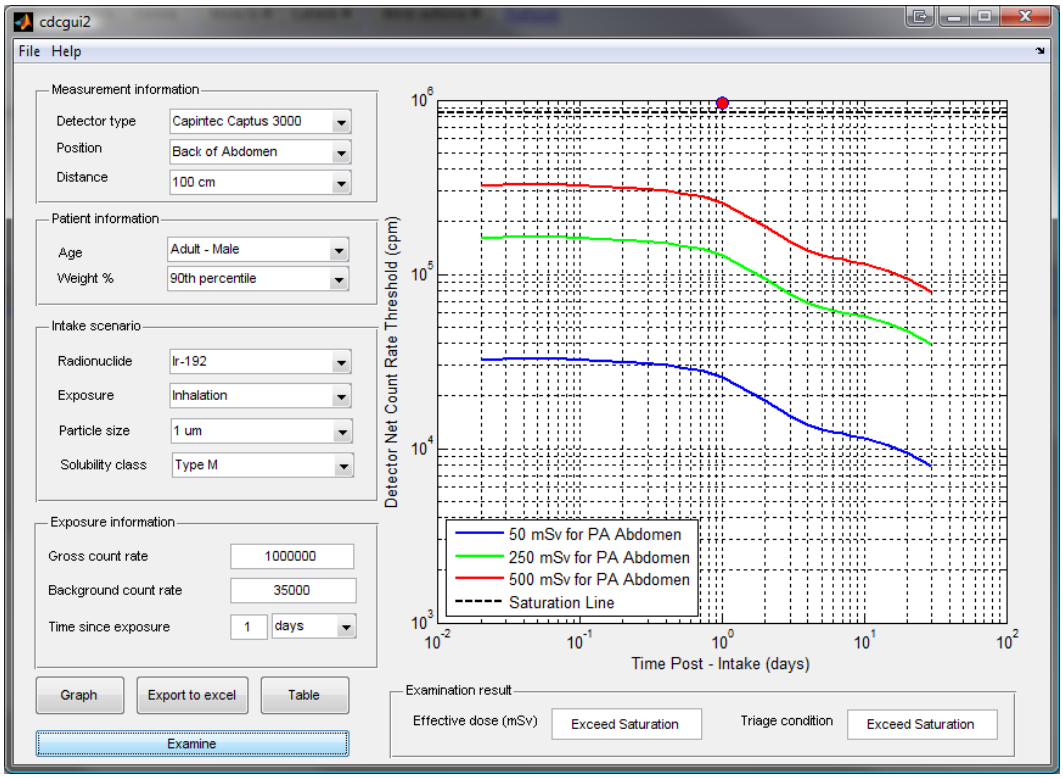

(B)

Figure 3-4. Triage condition assessment for Ir-192 Inhalation for the adult male with the Capintec Captus 3000 placed 100 cm away from the back of the abdomen reading gross count rate of (A) 225,000 cpm and (B) 1,000,000 cpm

CHAPTER 4
DISCUSSION

Variation in Count Rate Threshold by Detector Type

The time dependent detector count-rate threshold corresponding to a 250 mSv effective dose for an adult female (50^{th} weight percentile) for different detectors, except the Ludlum 12s, placed at the back chest (0 cm distance) is displayed in Figure 4-1a-e. The Ludlum 12s was excluded from this comparison, as its output is in different units than rest of the detectors. The Ludlum 12s uses μR/hr compared instead of cpm. Each figure corresponds to a different radionuclide with 1 μm AMAD particle size. The solubility class for each scenario is indicated in the caption. In all cases, the Canberra InSpector 1000 is shown to be the most sensitive detector, and the Ludlum 44-9 GM probe is the least sensitive detector. The other two detectors (the Ludlum 44-2 and the Capintec Captus 3000) show comparable results. The highest sensitivity of the Canberra InSpector 1000 can be credited to the 2 inch x 2 inch NaI crystal, which is four times as large as the Ludlum 44-2 detector used in this study. The Capintec Captus 3000 has a larger NaI crystal than the Ludlum 44-2, but due to this detector's limited solid angle it shows count rate comparable to this detector. Am-241 as seen in Figure 4-1a has the lowest counts of any radionuclide, and thus requires a high sensitivity detector such as the Canberra InSpector 1000. For Am-241 the Ludlum 44-9 is not recommended at any distance and the other four detectors should not be used at distance greater than 30 cm. If an individual has high internal contamination, Canberra InSpector is more likely to saturate due to higher sensitivity. In this case, the recommended solution is to place the detector further away from the body (at 30, 100,

or 200 cm) as necessary. However a less sensitive Ludlum 44-2 or 12s can also be used.

Variation in Count Rate Threshold by Subject Age and Gender

Figure 4-2 compares the detector net count rate threshold corresponding to a 250 mSv effective dose for all the age and gender combinations evaluated in the study. Only the 50th weight percentile phantoms were used for Adult male and female, for the variation in count rate threshold by weight percentile is discussed later. For this comparison, I-131 inhalation (1 μm AMAD with Type M solubility class) was assumed, and the Canberra Inspector 1000 spectrometer (placed 100 cm away from the back of the chest) was used for measurements. The figure shows that all age and gender combinations followed the expected pattern where net count rate threshold decreases with increasing time since exposure. The lowest counts were recorded for the 1 year old gender independent phantom, followed by 5 and 10 year old gender-independent phantoms. The 15 year old gender-dependent phantoms showed values higher than those estimated for 10 year olds, but lower than estimates for adults. The decrease in threshold count rate is a result of the ICRP effective dose coefficient, e, which decreases for the older individuals. This effect of the ICRP effective dose coefficient is offset to a certain degree by the decrease in the calculated Monte Carlo detector efficiency for the older individuals due to self-absorption. However, the effects of the ICRP effective dose coefficient are predominant.

Variation in Count Rate Threshold by Subject Weight Percentile

One of the primary goals of this study was to provide count rate thresholds that correspond to effective dose estimates for individuals with different body sizes. In this study, we chose to examine the two extremes (10th and 90th weight percentile

phantoms) for the U.S. population. Figure 4-3 shows the time dependent count rate threshold corresponding to 50 mSv estimated effective dose for adult males. The data is for the Ludlum 12s survey meter placed on the back surface of the individual's chest. The radionuclide, Cs-137, intake by inhalation with 1 μm AMAD particle size and Type F solubility class was assumed. The three different curves show almost identical behavior with the 10^{th} weight percentile phantom showing the highest counts and the 90^{th} weight percentile phantoms shows the lowest count. The 50^{th} weight percentile phantom lies in between the two as expected. The difference between the three comes from the self absorption of photons in the body of the individual. Thus the 10^{th} weight percentile phantom with the lowest volume for self-absorption within the body shows the highest count. Unfortunately, in the DCAL dataset the values of fractional retention are only given for gender-independent adult phantom, so all three phantoms were assumed to metabolize at the same rate. This remains the biggest limitation while comparing count rate threshold by subject's weight percentile, and could be a source of large uncertainty in our estimates of effective dose.

Analysis of the Monte Carlo Detector Efficiencies

To better understand the limitations of use for detectors used in this study with distance, radionuclide, and organ combinations, absolute detector Monte Carlo Efficiencies were plotted for all the eleven phantoms. A total of 500 graphs were generated for all possible combinations of fifty radionuclide and organ combinations, five detectors, and two anatomical positions. A representative graph is shown in Figure 4-4, which shows the Ludlum 44-2 results from back of the chest for the radionuclide Co-60 and organ small intestine content. In an ideal case, the behavior shown in the

figure will be depicted by all 500 graphs. The detector efficiencies vary when detector is closer to the individual and should converge at greater distances. Most of the data follows this pattern with some exceptions. The first deviation was noticed with radionuclide Am-241 at greater distances. The graphs verified that unlike other radionuclide, typically Am-241 does not converge at greater distances. The other significant deviation was seen from the Capintec Captus 3000 at contact. As shown in Figure 2-3, the Capintec Captus 3000 has a limited solid angle, so for certain combinations it does not detect all the photons emitted from an organ. This detector should not be used at contact because at such short distance the internal dose estimation will vary greatly with the placement of the detector on the body. The only other noticeable deviation comes from the organs ET1 and ET2 at shorter distances, especially with low energy emitting radionuclide, such as Am-241, or inefficient or limited-angle detector, such as the Ludlum 44-9 and Capintec Captus 3000. This is primarily due to placement on the detectors on the body (back of chest and abdomen), relatively farther away from extra thoracic region. The ET1 and ET2 contribution, however, are mostly an order of magnitude lower than the other organs, so they do not greatly influence the triage conditions.

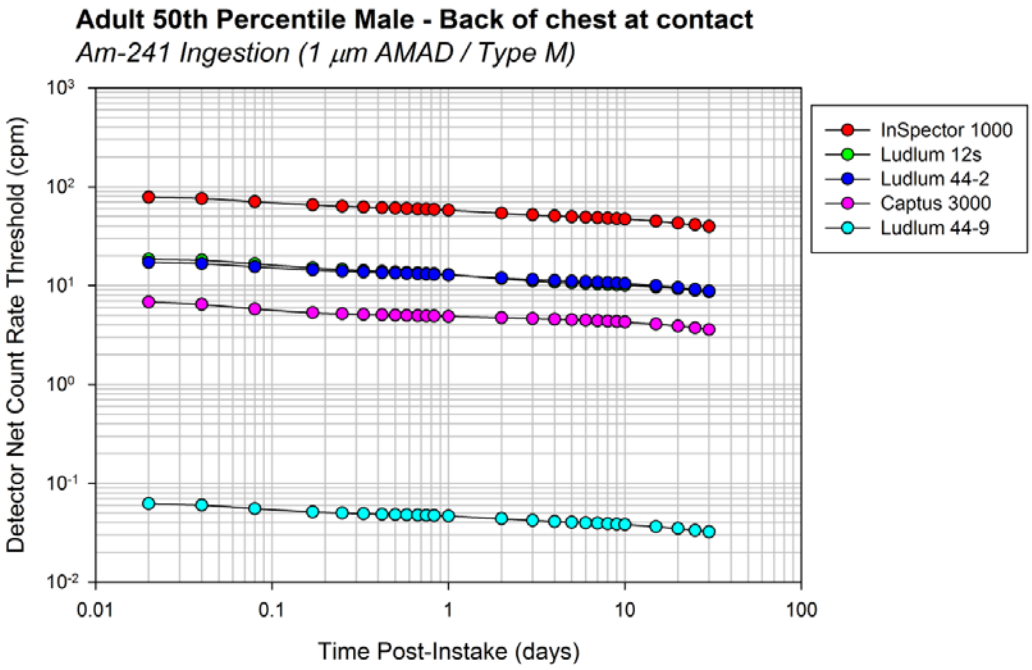

(A)

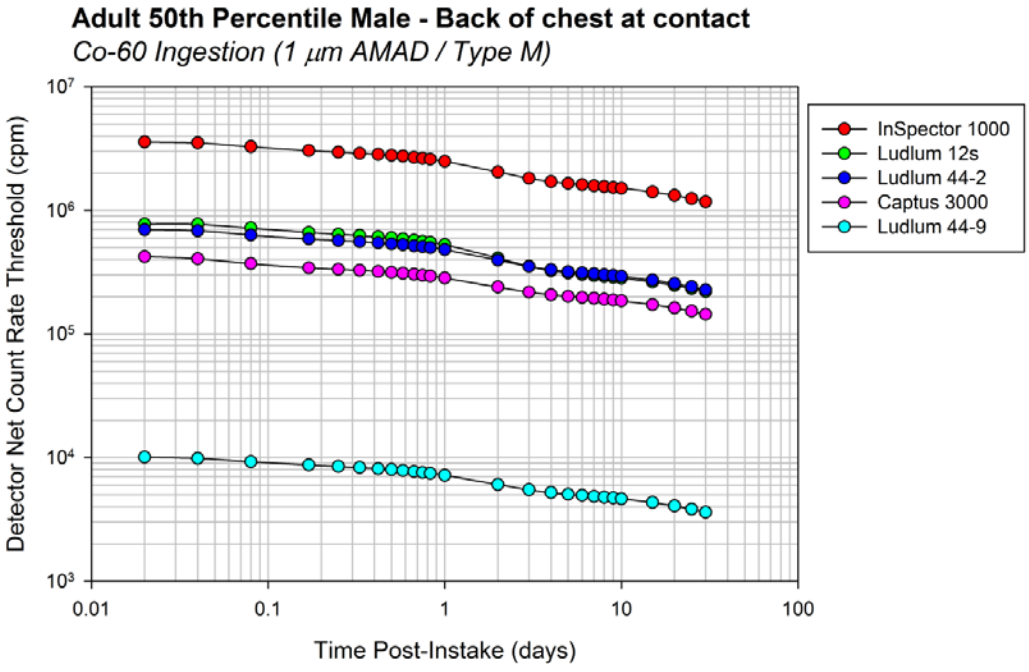

(B)

Figure 4-1. Comparison of 250 mSv count rate thresholds for the four survey meters for each radionuclide exposure scenarios assuming inhalation and default particle size and solubility type: A) Am-241, B) Co-60, C) Cs-137, D) I-131, and E) Ir-192 .

Figure 4-1. Continued.

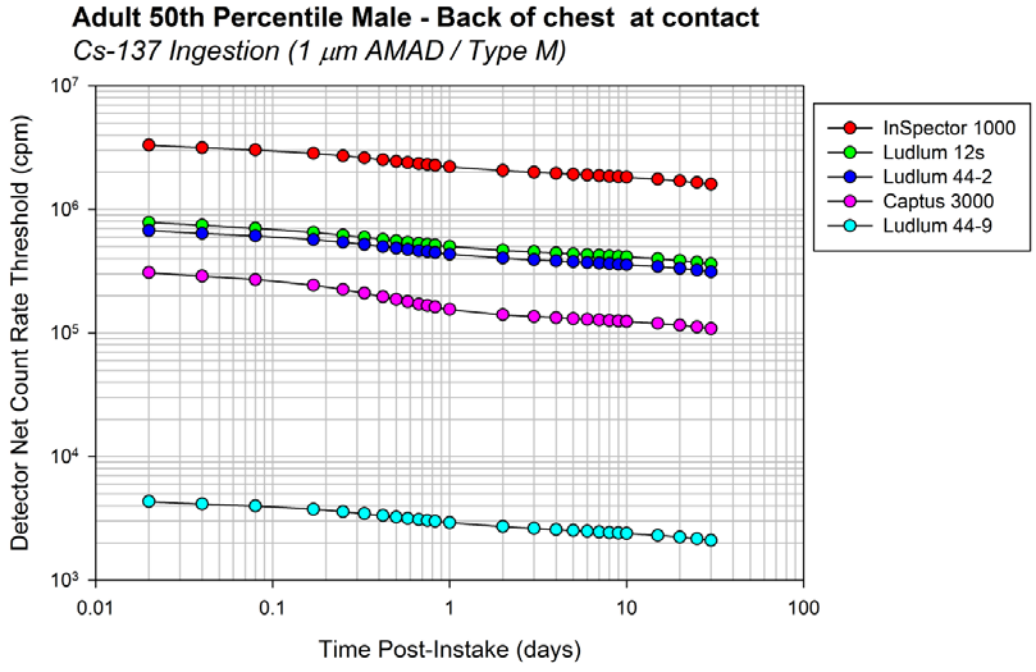

(C)

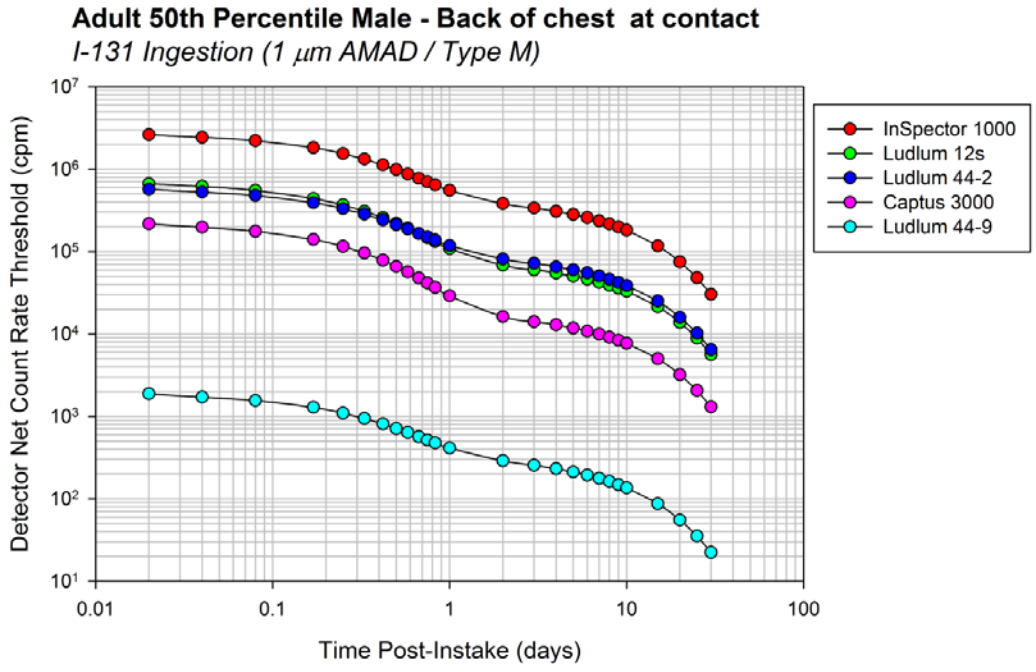

(D)

Figure 4-1. Continued.

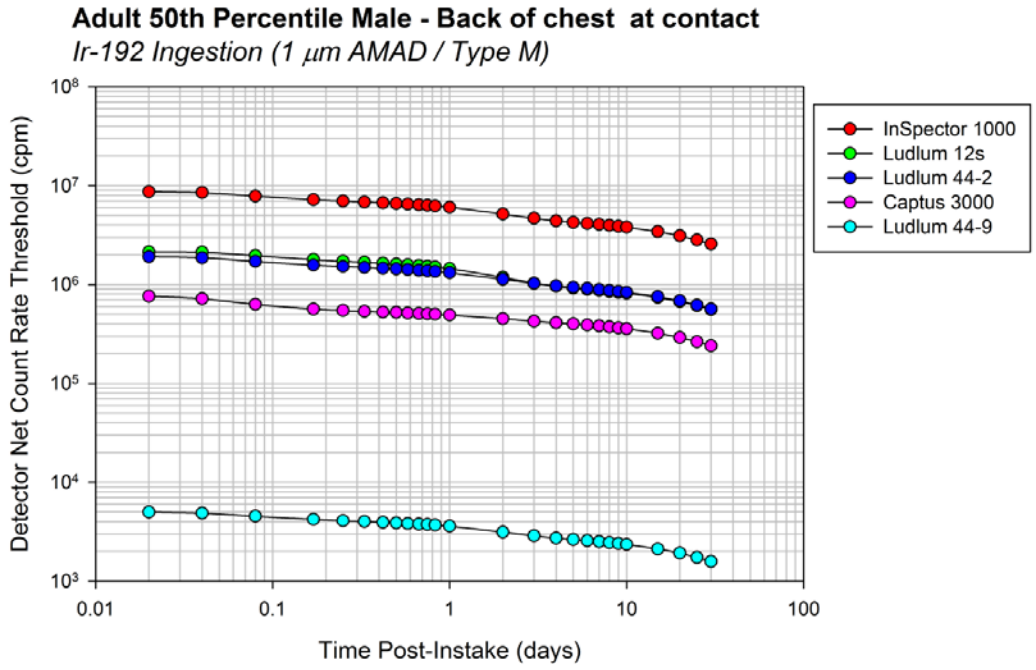

(E)

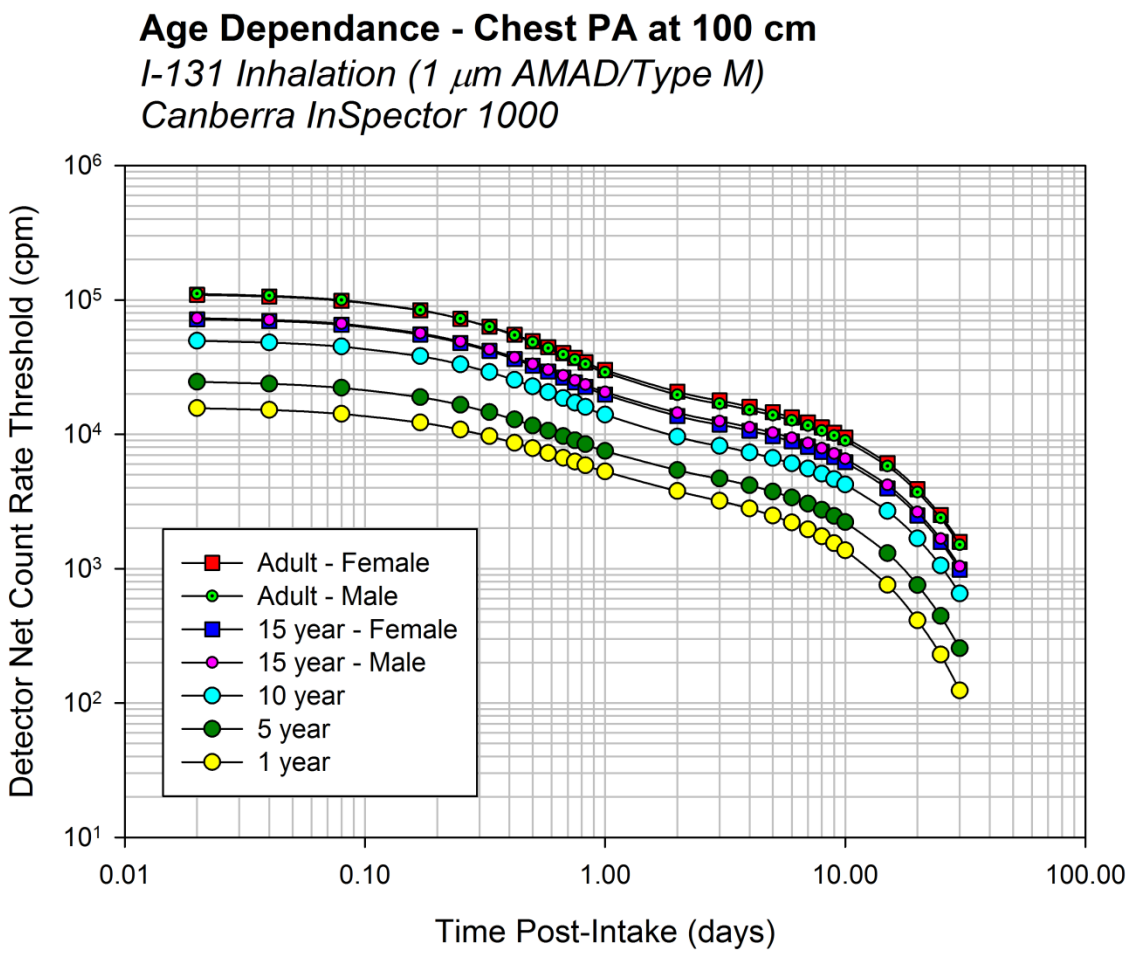

Figure 4-2. Comparison of 250 mSv count rate thresholds for all the age and gender combinations evaluated in this study assuming I-131 inhalation using the the Canberra InSpector 1000 spectrometer placed 100 cm away from the back of the chest.

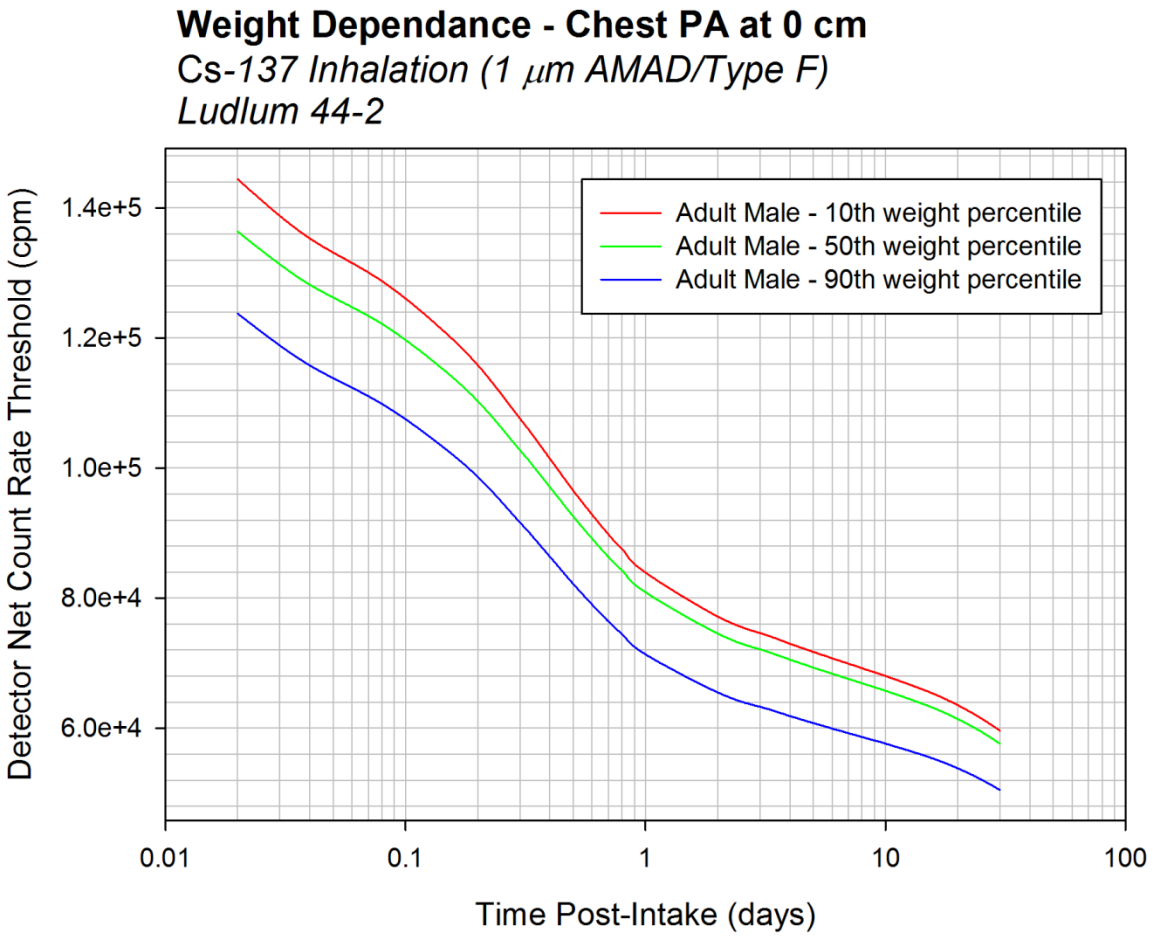

Figure 4-3. Comparison of 50 mSv count rate thresholds for the 10th, 50th, and 90th weight percentile adult male phantoms assuming Cs-137 inhalation using the Ludlum 44-2 survey probe placed at the back of the chest.

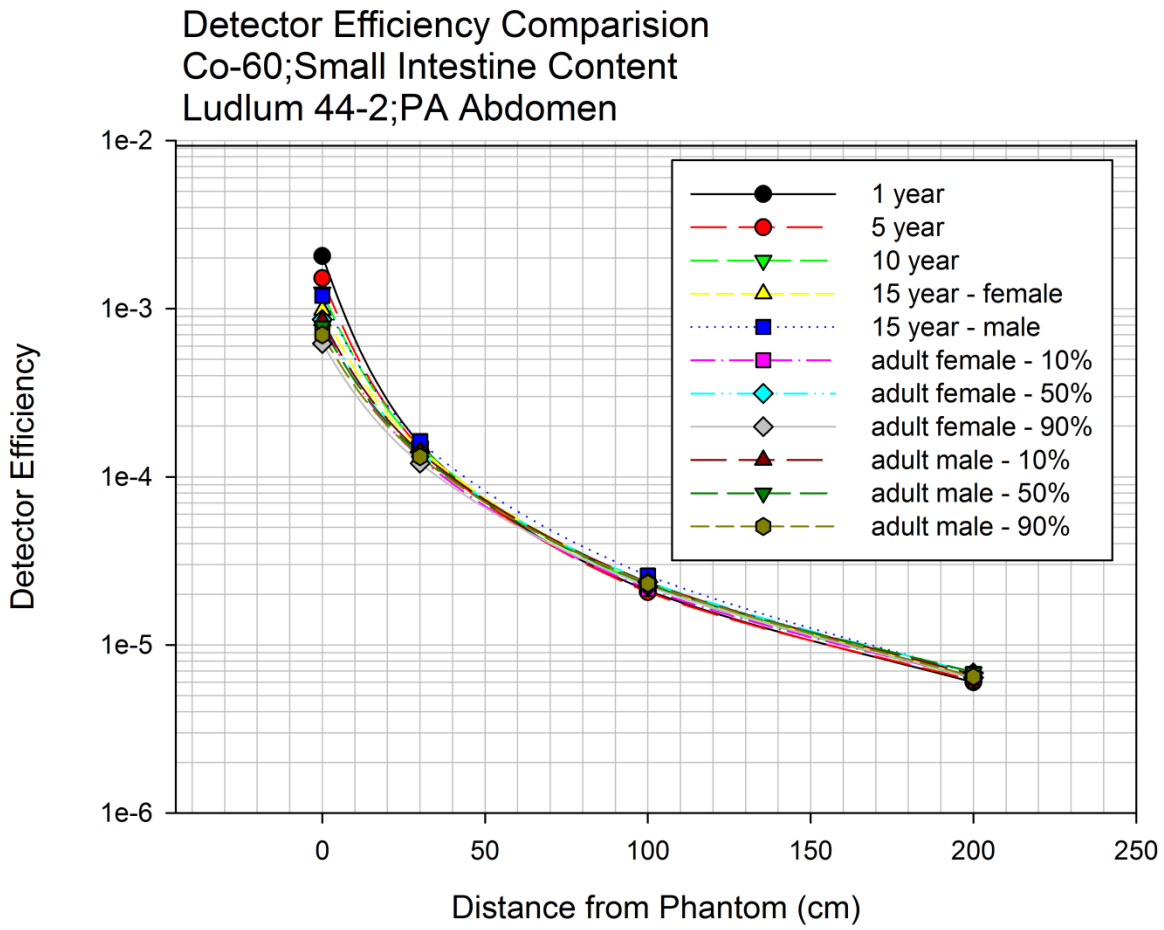

Figure 4-4. Comparison of absolutely Monte Carlo detector efficiency obtained for Co-60 radionuclide for organ small intestine content with the Ludlum 44-2 placed at the back of abdomen.

CHAPTER 5
CONCLUSION

After a large scale RDD event, with thousands of potentially contaminated individuals to screen for internal contamination, there is a dire need for a rapid triage method using readily available tools. In this study, we evaluated the use of portable survey meters to estimate the internal contamination of any individual for five radionuclide of interest: Am-241, Co-60, Cs-137, I-131, Ir-192. For these radionuclides, based on the availability of the ICRP effective dose coefficients, 21 combinations of inhalation and ingestion scenarios were considered. The contaminated individuals were simulated in a Monte Carlo based program MCNPX using hybrid computational phantoms of a different age, gender, and weight percentile. The end result of the current study was an intuitive MATLAB based Graphical User Interface that is capable of showing the results in either graphical or tabular format, as well as evaluating the triage conditions. There are four possible triage conditions corresponding to doses of: less than 50 mSv, between 50 and 250 mSv, between 250 and 500 mSv, and greater than 500 mSv. This triage condition can be calculated using any of the five detectors used in the study: The Ludlum 44-2, Ludlum 44-9, Ludlum 12s, Capintec Captus 3000, and Canberra Inspector 3000. These detectors can be placed either at the back of the chest or abdomen of the potentially contaminated individual at 0, 30, 100, or 200 cm away.

It should be emphasized that the intent of this method is not to predict the definitive internal contamination, but to help with quick triage. The estimates of the internal contamination of the individual are subject to various uncertainties. The key assumption is that the individual has little or no external contamination. This sometimes may be the case, but the triage conditions will be more conservative in these rare

scenarios. Also, the results of 10^{th} and 90^{th} weight percentile phantoms are still limited by the reference Biokinetic models and ICRP effective dose coefficient. This study also requires knowledge of the radionuclide used in the event, and only one radionuclide can be evaluated at a time. Future studies will concentrate on allowing this method of triage readily available at any remote site. This includes a conversion from the PC-based software to a PDA-software and the ability to use virtually any portable survey device to make triage decisions.

APPENDIX A
EXCEL OUTPUT OF THE SOFTWARE

Table A-1. Excel output from the PC-based MATLAB GUI

Measurement Information			
Detector Type	Capintec Captus 3000		
Position	Abdomen PA		
Distance	30 cm		
Patient Information			
Age	Adult - Male		
Weight %	90th percentile		
Intake Scenario			
Radionuclide	Ir-192		
Exposure	Inhalation		
Particle Size	1 um		
Solubility Class	Type M		
Time (days)	50 mSv	250 mSv	500 mSv
0.02	55125.43	275627.1	551254.3
0.04	61752.82	308764.1	617528.2
0.08	63541.79	317708.9	635417.9
0.17	62218.42	311092.1	622184.2
0.25	60492.97	302464.8	604929.7
0.33	59027.74	295138.7	590277.4
0.42	57331.19	286655.9	573311.9
0.5	55556.39	277781.9	555563.9
0.58	54014.29	270071.4	540142.9
0.67	52229.32	261146.6	522293.2
0.75	50546.13	252730.7	505461.3
0.83	48808.91	244044.5	488089.1
1	45145.29	225726.5	451452.9
2	27142.73	135713.7	271427.3
3	17946.27	89731.34	179462.7
4	13988.63	69943.13	139886.3
5	12375.71	61878.54	123757.1
6	11584.59	57922.93	115845.9
7	11216.51	56082.53	112165.1
8	10950.17	54750.83	109501.7
9	10737.51	53687.55	107375.1
10	10553.63	52768.13	105536.3
15	9699.434	48497.17	96994.34
20	8966.612	44833.06	89666.12
25	8312.487	41562.44	83124.87
30	7742.289	38711.44	77422.89

LIST OF REFERENCES

Booth TE, Hughes HG, Zukaitis A, Brown FB, Mosteller RD, Marsha Boggs C, Bull JS, Prael RE, Forster RA, Sood A, Goorley JT, Sweezy JE. MCNP — A General Monte Carlo N-Particle Transport Code, Version 5 Volume II: User's Guide. Los Alamos, NM: Lost Alamos National Laboratory LA-CP-03-0245; 2003.

CRCPD. Handbook for responding to a radiological dispersal device [online]. Available at: http://www.crcpd.org/RDD_Handbook/RDD-Handbook-ForWeb.pdf. Accessed Feb 20 2011.

DOE/NRC. Radiological Dispersal Devices: An initial study to identify radioactive materials of greatest concern and approaches to their tracking, tagging, and disposition [online]. Available at: http://www.nti.org/e_research/official_docs/doe/DOE052003.pdf. Accessed June 18th 2010.

Eckerman K, Endo A. MIRD: Radionuclide Data and Decay Schemes. 1st ed. The Society of Nuclear Medicine; 2008.

Elcock D, Klemic GA, Taboas AL. Establishing Remediation Levels in Response to a Radiological Dispersal Event. Environmental Science & Technology 38: 2505-2512; 2004.

Gonzalez AJ. Security of radioactive sources: threats and answers. International Conference on Security of Radioactive Sources 33-58; 2003.

ICRP. Age-dependent Doses to the Members of the Public from Intake of Radionuclides - Part 5 Compilation of Ingestion and Inhalation Coefficients. Pergamon Press.; 1995.

ICRP. Basic anatomical and physiological data for use in radiological protection: reference values: ICRP Publication 89. Pergamon Press.; 2002.

Johnson PB, Whalen SR, Wayson M, Juneja B, Lee C, Bolch WE. Hybrid patient-dependent phantoms covering statistical distributions of body morphometry in the u.s. adult and pediatric population. Proceedings of the IEEE 97: 2060-2075; 2009.

Lee C, Lodwick D, Hurtado J, Pafundi D, Williams JL, Bolch WE. The UF family of reference hybrid phantoms for computational radiation dosimetry. Physics in Medicine and Biology 55: 339-363; 2010.

Lee C, Lodwick D, Williams JL, Bolch WE. Hybrid computational phantoms of the 15-year male and female adolescent: Applications to CT organ dosimetry for patients of variable morphometry. Medical Physics 35: 2366-2382; 2008.

Maiello ML, Groves KL. Resources for nuclear and radiation disaster response. Nuclear News 49: 29-34; 2006.

NCRP. Management of persons contaminated with radionuclides: Handbook. Bethesda, MD: National Council on Radiation Protection and Measurements. Report No. 161; 2008.

NCRP. Responding to a radiological or nuclear terrorism incident: A guide for decision makers. Bethesda, MD: National Council on Radiation Protection and Measurements. Report No. 165; 2010.

NRC US. Background on Dirty Bombs [online]. Available at: http://www.nrc.gov/reading-rm/doc-collections/fact-sheets/dirty-bombs-bg.html. Accessed February 20 2011.

NRT US. Reconciling federal emergency response plans – NRT homeland security recommendations [online]. Available at: http://www.nrt.org/production/NRT/NRTWeb.nsf/AllAttachmentsByTitle/A-60RFERPorRechs/$File/rechs.pdf?OpenElement. Accessed Feb 20 2011.

Pelowitz D. MCNPX User's Manual Version 2.5.0. Los Alamos, NM: Lost Alamos National Laboratory LA-CP-05-0369; 2005.

Smith JM, Ansari A, Harper FT. Hospital Management of Mass Radiological Casualties: Reassessing Exposures From Contaminated Victims of An Exploded Radiological Dispersal Device. Health Physics 89: 513-520; 2005.

Sohier A, Hardeman F. Radiological Dispersion Devices: Are we prepared? Journal of Environmental Radioactivity 85: 171-181; 2006.

BIOGRAPHICAL SKETCH

Mr. Juneja received his Bachelor of Science degree in nuclear engineering from the Nuclear and Radiological Department at the University of Florida. He received his Master of Science degree in medical physics at the University of Florida. He is a member of the American Associates of Physicists in Medicine (AAPM) and served as a President of Alpha Nu Sigma Florida chapter and Vice-president of American Nuclear Society (ANS) Florida student section. His research interests include development of hybrid human phantom and radiation dosimetry calculations for IMRT and Proton based radiation therapy utilizing reference phantoms and Monte Carlo transport methods.